THE ACTIVITY OF ZnO IN THE TERNARY SYSTEM $ZnO-CaO-SiO_2$

by

MICHAEL JOHN FAIRWEATHER

A THESIS SUBMITTED IN PARTIAL FULFILMENT

OF THE REQUIREMENTS FOR THE DEGREE OF

MASTER OF APPLIED SCIENCE

IN THE DEPARTMENT

OF

METALLURGY

We accept this thesis as conforming to the

standard required from candidates for

the degree of MASTER OF APPLIED SCIENCE

Members of the Department of Metallurgy

THE UNIVERSITY OF BRITISH COLUMBIA

February, 1967.

In presenting this thesis in partial fulfilment of the requirements for an advanced degree at the University of British Columbia, I agree that the Library shall make it freely available for reference and study. I further agree that permission for extensive copying of this thesis for scholarly purposes may be granted by the Head of my Department or by his representatives. It is understood that copying or publication of this thesis for financial gain shall not be allowed without my written permission.

Department of Metallurgy

The University of British Columbia
Vancouver 8, Canada

Date February 7, 1967

ABSTRACT

The activity of ZnO in ternary Zno-CaO-SiO_2 slags has been measured at 1300 C by equilibration with copper rich brass and low oxygen potential gas utilizing the following reversible galvanic cell:

$$Pt \mid H_2, H_2O \parallel 0.85ZrO_2\text{-}0.15CaO \parallel O_{2(Air)} \mid Pt$$

Thermodynamic data on the component binaries was employed to calculate the excess free energy of the ternary system and the isoactivity patterns of the three components at 1600 C with respect to the metastable pure liquid standard states. An estimate of 6 E.U. was made for the entropy of fusion of ZnO. The measured activities are in good agreement with the calculated values.

The proposed excess free energy contours in the ZnO-CaO-SiO_2 ternary are similar in shape to those calculated in a similar manner for the FeO-CaO-SiO_2 system. Also the calculated zinc oxide isoactivity figure resembles the ferrous oxide isoactivity diagram. This zinc oxide isoactivity pattern projects towards the lime orthosilicate composition. This shape is characteristic of FeO, but in the case of ZnO the projection is less pronounced. Both these observations are in keeping with the slightly more basic behaviour of zinc oxide.

ACKNOWLEDGEMENT

The author would like to extend his sincere thanks to his research director, Dr. C. S. Samis for his continued encouragement and guidance throughout this work. The explanations and contributions by Dr. G. W. Toop and Dr. W. G. Davenport are greatly appreciated. The help and interest shown by various members of the faculty, staff and especially fellow graduate students is warmly acknowledged.

Appreciation is expressed to the Defence Research Board and the National Research Council of Canada whose financial support made this work possible.

TABLE OF CONTENTS

TABLE OF CONTENTS (continued)

TABLE OF CONTENTS (continued)

LIST OF FIGURES

LIST OF FIGURES (continued)

LIST OF TABLES

THE ACTIVITY OF ZnO IN THE TERNARY SYSTEM ZnO-CaO-SiO_2

INTRODUCTION

A. General

Zinc oxide bearing slags have industrial importance. In several metallurgical processes the zinc oxide in these slags is selectively reduced in fuming furnaces to recover the zinc values. As the fuming rates of zinc oxide are directly related to its activity in a slag, studies of the activity of zinc oxide in various slags have an economic justification.

B. Previous Work

Bell, Turner and Peters[3] calculated the activities of zinc oxide from operating plant data in several slags from an operating lead blast furnace. In this particular process the furnaces operate at approximately 1200°C and utilize slags containing a maximum of 25 percent ZnO. These calculations were done with respect to solid zinc oxide and for slags of constant CaO to SiO_2 + Al_2O_3 ratio.

Richards and Thorne[4] equilibrated FeO-CaO-SiO_2 and FeO-SiO_2 melts containing one to two percent ZnO in iron boats with a CO-CO_2 gas containing zinc vapour. They found that the ternary system ZnO-FeO-SiO_2 could be represented by a regular solution approximation in which the interaction energy between zinc oxide and ferrous oxide was assumed to be zero.

The most recent work, by Azuma et. al.[6], reports activities of zinc oxide in slags containing iron oxide, saturated and unsaturated with silica, as a function of lime content. They state that for silica saturated slags, γ_{ZnO} remains constant at about 1 with increasing CaO, while for slags not saturated in silica, γ_{ZnO} increases from 1.8 to 3.1 with an increase in the CaO content from zero to 16.5 weight percent. Unfortunately information on the zinc oxide contents, the experimental temperatures and the entropy of fusion used for zinc oxide is unavailable at the present time.

The most extensive investigation available is by Davenport[5] who determined activities in the $ZnO-FeO-SiO_2$ ternary and $ZnO-FeO-SiO_2-CaO$ quaternary. He also calculated activities in the $ZnO-CaO-SiO_2$ ternary using Elliott's[7] information on the $FeO-CaO-SiO_2$ system. In order to determine the activity of zinc in the system he used an iron saturated brass held in an iron curcible. The resulting Fe-FeO equilibria determined the oxygen potential and hence the range of zinc oxide activity available was limited. It was felt that this work might be extended if a means could be found to remove this limitation.

C. Scope of Present Investigation

The ternary $ZnO-CaO-SiO_2$ is the simplest slag system containing zinc oxide with a wide range of acid-base behaviour. Based on the similarity between the free energies, with respect to the solid standard state, of the two oxides FeO and ZnO with silica[8], this system should resemble the $FeO-CaO-SiO_2$ ternary. The $ZnO-CaO-SiO_2$ ternary has a somewhat limited area with a melting point under 1300°C[2]. It is proposed to use the simple equilibrium

$$Zn_{(l)} + 1/2O_{2(g)} \rightleftharpoons ZnO_{(s)} \qquad \ldots(1a.)$$

for which

$$K_{1573^{\circ}K} = 7.3 \times 10^{-7} \ (9) \qquad \ldots(1b.)$$

to determine zinc oxide activities in slags from this ternary, primarily along the line of silica saturation at 1300°C.

D. Experimental Method

In order to thermodynamically fix the activity of zinc oxide in a slag it is necessary to measure the oxygen potential and the zinc activity. In appendix I a discussion is given of the available information on the copper-zinc binary. For low concentration of zinc the following approximate expression is derived.

$$\overline{\Delta F}_{Zn}^{xs} = -8200 + 2.58\ T \qquad \ldots (2)$$

Hence the activity coefficient for zinc will be less than unity. It is also possible to directly measure the oxygen potential of a gas phase using an oxygen solid electrolyte of the type to be described in section II. The activity of zinc oxide in a slag may be measured by the zinc content of a copper rich brass and the oxygen potential of gas when both are in equilibrium with a ZnO bearing slag.

THERMODYNAMIC MEASUREMENT BY OXYGEN HALF-CELLS

A. Theory of Oxygen Solid Electrolytes

1) Defect Structure

Hund[10] first showed that oxide mixtures containing a predominance of valence IV metallic ion with a small percentage of valence II or III metallic ion should be capable of acting as solid oxygen electrolytes. Due to the oxygen ion mobility in the oxygen ion deficient lattice structure, under certain conditions

(temperature and oxygen partial pressure) oxygen ion transport is the major conduction mechanism. Kuikkola and Wagner[11] made several of these oxide mixtures at varying composition and showed that at certain conditions, many of these structures do conduct almost entirely by oxygen ion transport.

Zirconium dioxide forms an anion vacancy type of lattice. This is known from measurements of conductivity and oxidation rate as a function of oxygen partial pressure. In the pure zirconia ionic lattice (Figure 1a) as oxygen ions are removed, free electrons are formed. In the pure material the concentration of these defects is relatively small. The addition of a lower valence impurity oxide such as lime or yttria to this structure will cause a proportional increase in the number of anion defects to keep the cation to anion charge balance within the original structure. For every calcium ion that enters the lattice on a zirconium ion site there will be an oxygen vacancy formed without increasing the number of free electrons. (Figure 1b).

2. Conduction Mechanism

In a pure oxide of this type (anion deficient) at low oxygen partial pressure the conduction reaction will be:

$$1/2\ O_2 + O_{\square}^{++} + 4\,e^- \rightleftharpoons O^{=} \qquad \ldots (3)$$

As the oxygen partial pressure is increased the oxide tends to approach stoichiometry. At high oxygen partial pressure oxygen ion interstitials together with electron holes will be formed.

$$1/2\ O_2 \rightleftharpoons O_I^{=} + 2\oplus \qquad \ldots (4)$$

Conductivity is due to three charge carriers in any combination: oxygen ions, free electrons and positive electron holes

$$\sigma_T = \sigma_{ion} + K_1 PO_2^{1/n} + K_2 PO_2^{-1/m} \ (12) \qquad \ldots (5)$$

where K_1, K_2, n and m are constants.

$$\begin{array}{cccc} Zr^{+4} & O^{=} & O^{=} & Zr^{+4} \\ e^{-} & & & \\ O^{=} & Zr^{+4} & O^{=} & O^{=} \\ O^{=} & \square^{++} & Zr^{+4} & O^{=} \\ & & e^{-} & \\ Zr^{+4} & O^{=} & O^{=} & Zr^{+4} \end{array}$$

Figure 1a. Pure Zirconium Dioxide.

$$\begin{array}{cccc} Zr^{+4} & O^{=} & O^{=} & Zr^{+4} \\ O^{=} & Ca^{+2} & O^{=} & O^{=} \\ O^{=} & O^{=} & Zr^{+4} & O^{=} \\ Zr^{+4} & \square^{++} & O^{=} & Zr^{+4} \\ O^{=} & Zr^{+4} & O^{=} & O^{=} \end{array}$$

Figure 1b. Zirconium Dioxide with Calcium Oxide Addition

With increasing oxygen partial pressure conductivity owing to positive hole conduction will increase and conductivity due to electron conduction will decrease (Figure 2).

With oxide mixtures of the zirconia-yttria, zirconia-lime types, there are large numbers of vacant oxygen sites which are uncharged. Conductivity reactions then occur as in figure 3. If the contribution of charge carried by the electrons in the oxide is negligible with respect to that carried by oxygen ions then the transport number for oxygen ions may be taken as unity. Steele and Alcock[13] indicate that both lime and yttria stabilized zirconia would be useful for the range of oxygen potential to be used in the present study.

B. Criteria for Reversibility

The determination of chemical potential by emf methods is based on the Nernst equation.

$$-nFE = \Delta F$$

This applies to a chemical reaction having a Gibbs free energy ΔF when carried out reversibly in an electrochemical cell. E is the electromotive force generated, n is the number of electrons transported by the reaction and F is the Faraday constant. The emf of the cell

$$Pt,\ O_2\ (\mu_1)\ |\ 0.85ZnO_2\text{-}0.15CaO\ |\ O_2\ (\mu_2),\ Pt$$

is given exactly by

$$E = \frac{1}{4F}\int_{\mu_1}^{\mu_2} t_o^{-2}\, d\mu \qquad \ldots (7)$$

Here t_o^{-2} is the transport number of oxygen ions in the electrolyte. In the simple case where $t_o^{-2} = 1$ equation 7 reduces to

$$E = \frac{1}{4F}\ (\mu_2 - \mu_1) \qquad \ldots (8a)$$

$$E = \frac{RT}{4F} \ln \frac{a_o^{-2}\ II}{a_o^{-2}\ I} \qquad \ldots (8b)$$

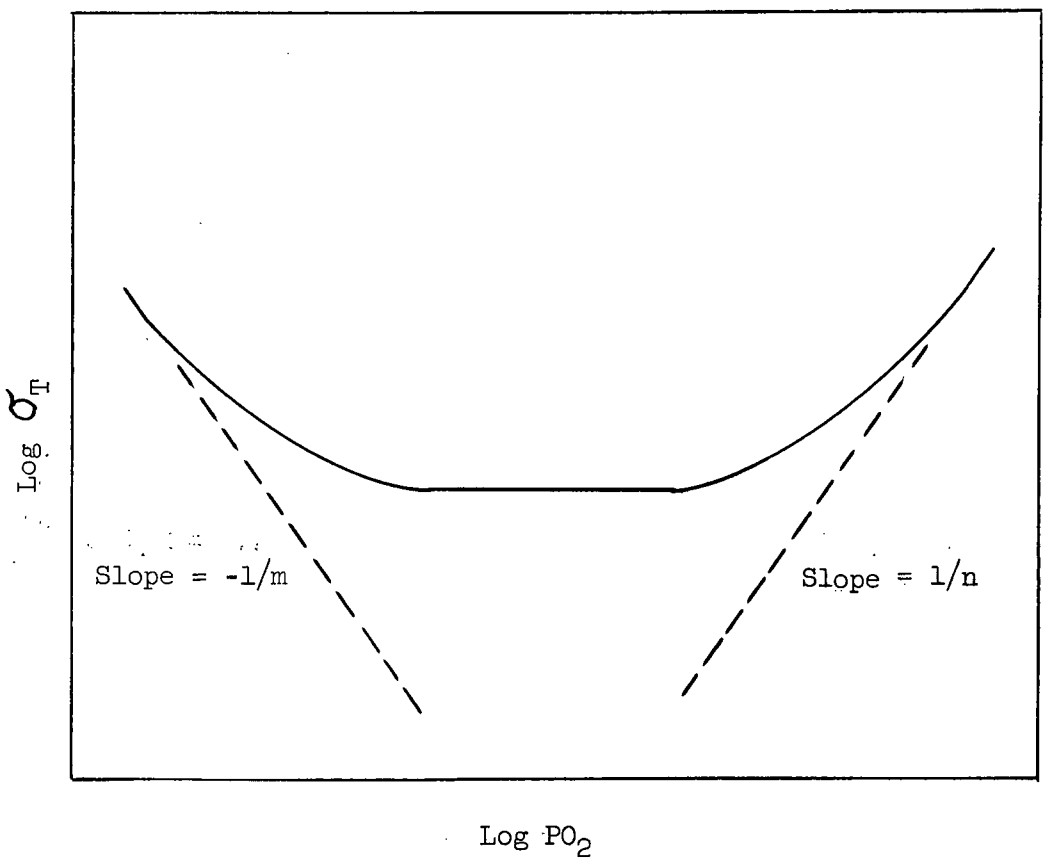

Figure 2. Oxide conductivity as a Function of Oxygen Partial Pressure[14].

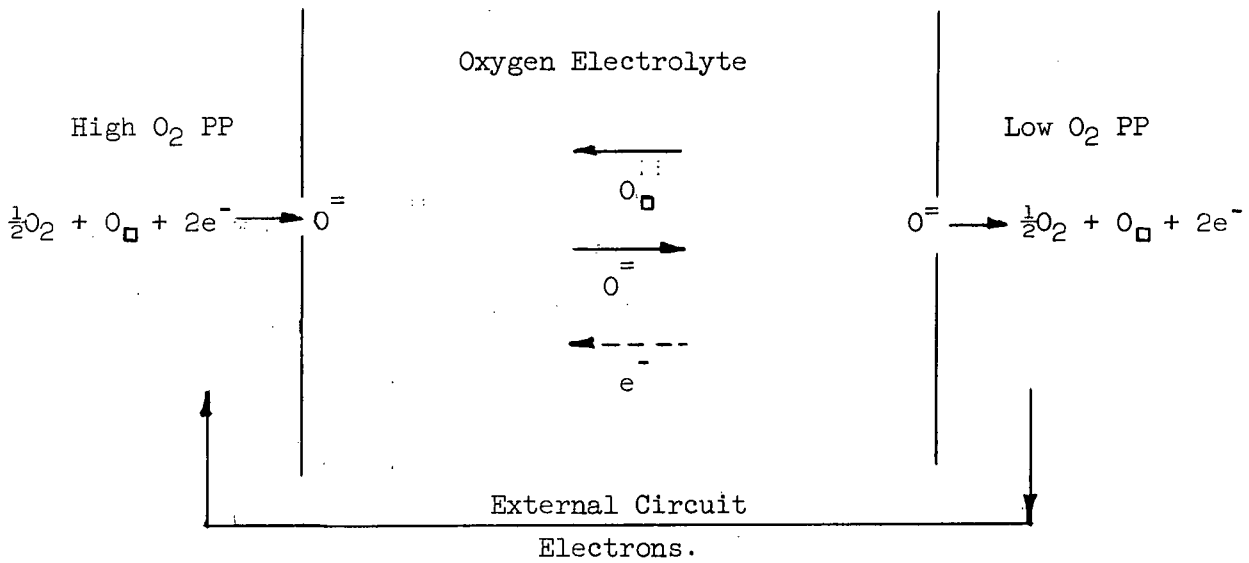

Figure 3. Conductivity Reactions at Cathode and Anode in an Oxygen Electrolyte with a Large Concentration of Oxygen Ion Vacancies.

This means that the cell functions as a simple concentration cell for oxygen potential.

THERMODYNAMIC CALCULATIONS

Toop[15] has shown that a simple proportional combination of the excess properties in the component binaries may adequately describe the excess properties in the ternary system. He has successfully applied this technique in the $FeO-CaO-SiO_2$ ternary[16] to calculate the excess free energy at 1600°C based on the pure liquid metastable standard states. It is shown (Appendix III) that from the α plots ($RT\ln \gamma i/(1-N_i)^2$ versus Ni) for each component in its binaries, the activities and excess free energies may be calculated.

A. Binary Oxide Systems

1.) $CaO-SiO_2$

Elliott[7] gives the excess free energy curve for the $CaO-SiO_2$ binary based on the metastable pure liquids (Figure 4). Tangent intercepts were taken from this curve to determine the α plots for the two components.

2.) ZnO-CaO

No information is available on the ZnO-CaO binary. As an approximation it is assumed that the α curve for FeO-CaO[7] may be used for the ZnO-CaO binary.

$$\alpha = \frac{RT\ln \gamma ZnO}{(1-N_{ZnO})^2} = \frac{RT\ln \gamma CaO}{(1-N_{CaO})^2} = -8580 \text{ cals mol}^{-3}$$

This assumption gives the simplest shape for the excess free energy, a simple parabola.

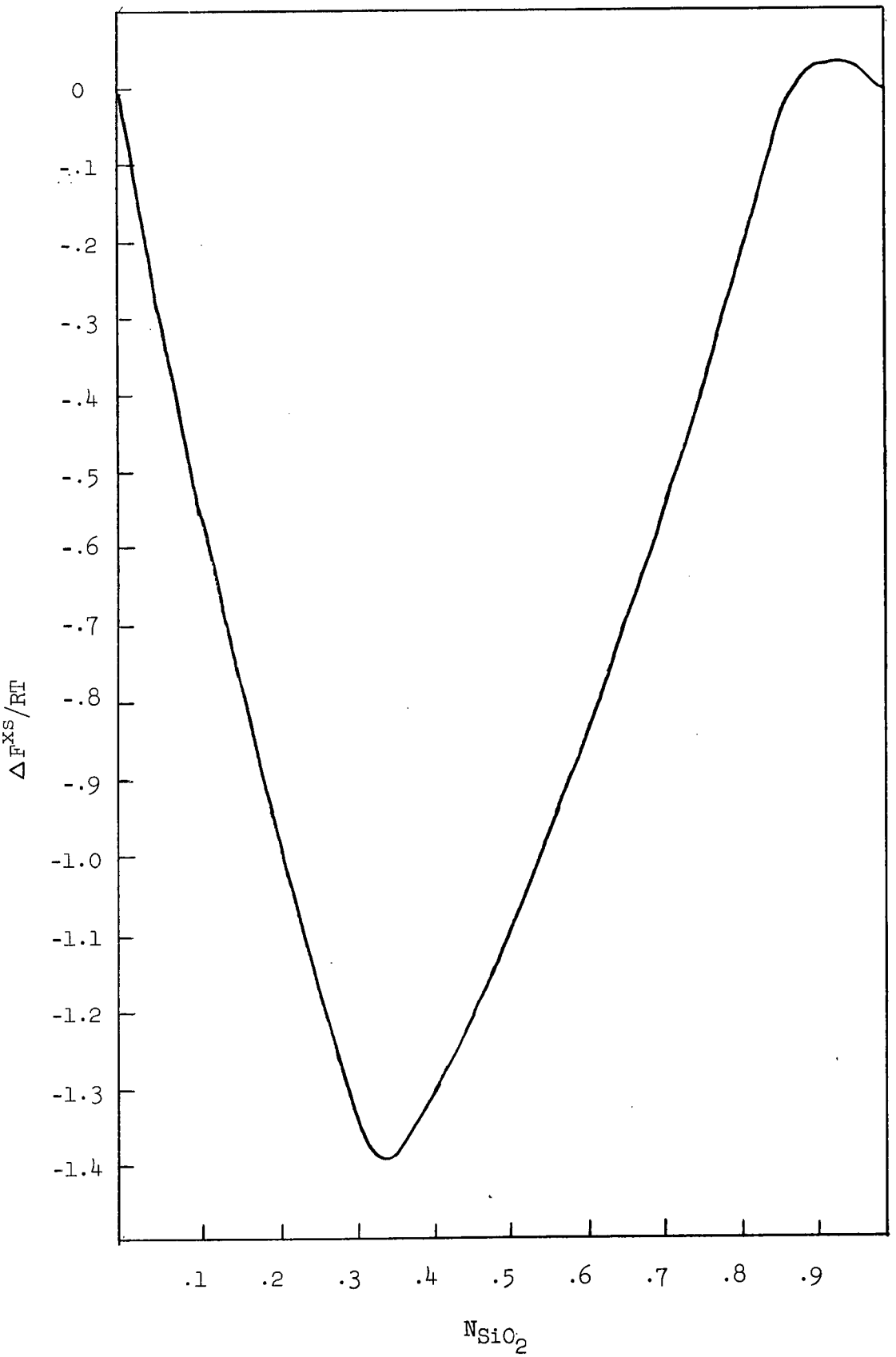

Figure 4. Excess Free Energy of the $CaO\text{-}SiO_2$ Binary at 1600°C Based on the Metastable Pure Liquid Standard States[7].

3.) $ZnO-SiO_2$

In order to derive suitable α plots for the $ZnO-SiO_2$ binary it is necessary to know activities of the two components relative to the metastable pure liquids at 1600°C. Bunting[1] has shown the phase diagram consists of a congruent melting compound, zinc orthosilicate, together with two simple eutectics (76.5 and 50 mol % ZnO) and a two phase liquid region at the silica rich side of the binary (Figure 5).

Activities may then be calculated from this phase diagram using Chipman's melting point depression method[18] and Hauffe and Wagner's congruent melting compound technique[19].

The following thermodynamic information was used:

1.) Entropy of fusion of silica (Cristobalite) estimated at 1.8 E.U.[17]

2.) Kitchener and Ignatowitz's[20] estimated heat of fusion for zinc orthosilicate of 18.7 Kcals/mol^{-1}.

3.) An entropy of fusion for zinc oxide of 6 E.U. estimated from Elliott's[26] activity diagram for the $ZnO-SiO_2$ binary. This calculation and the derivation of mutually compatible α curves based on the Duhem Margules equation[21] is given in appendix II. The excess free energy curve for the $ZnO-SiO_2$ binary is shown in figure 6.

B. $ZnO-CaO-SiO_2$ Ternary

A Fortran computer program was written for processing the binary data according to the equations developed in appendix III on the University IBM 7040 computer.

The excess free energy of the $ZnO-CaO-SiO_2$ ternary is given in figure 7 and the calculated isoactivity lines for the three components ZnO, SiO_2 and CaO are presented in figures 8, 9 and 10 respectively.

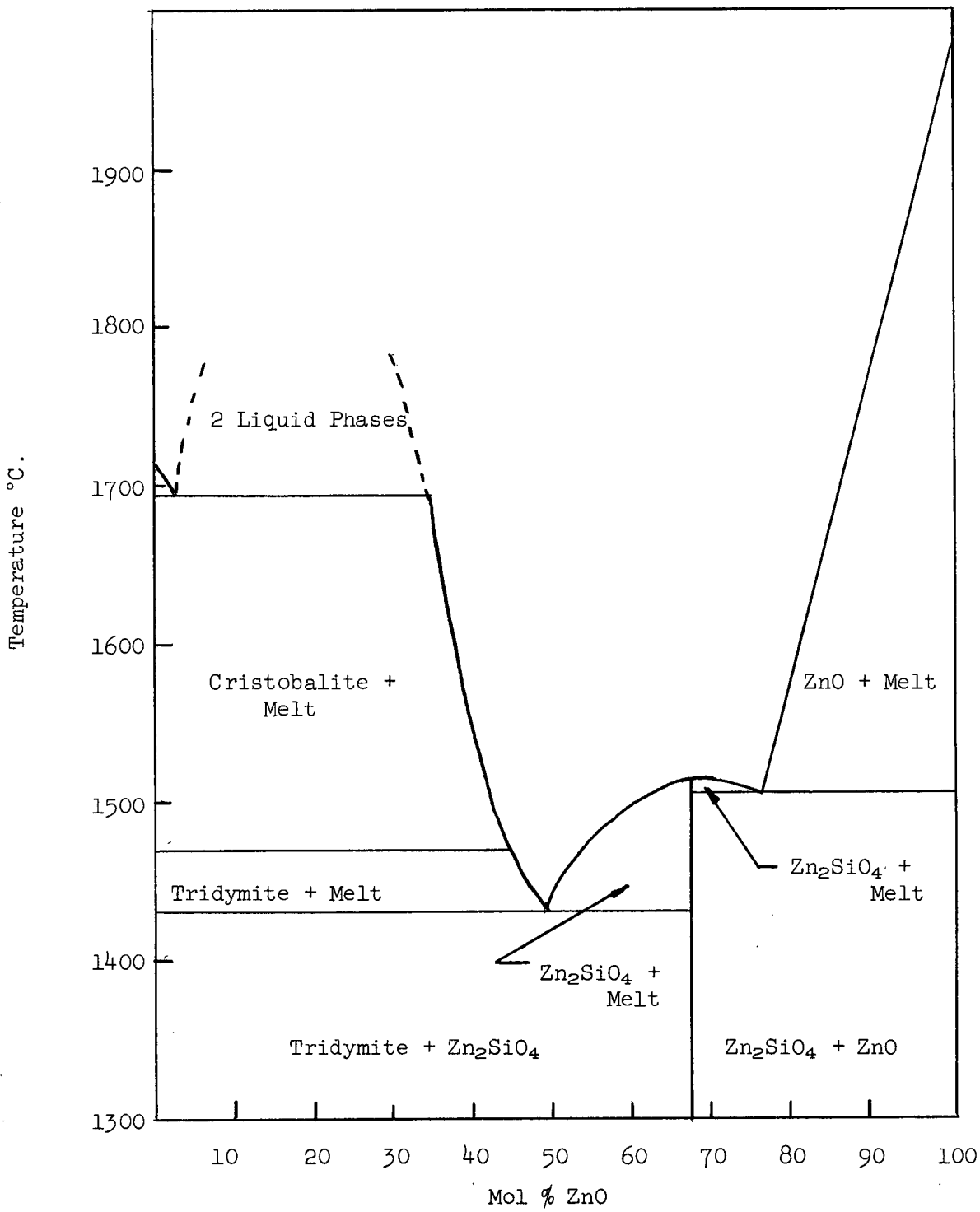

Figure 5. Phase Diagram, ZnO-SiO_2 System.[1]

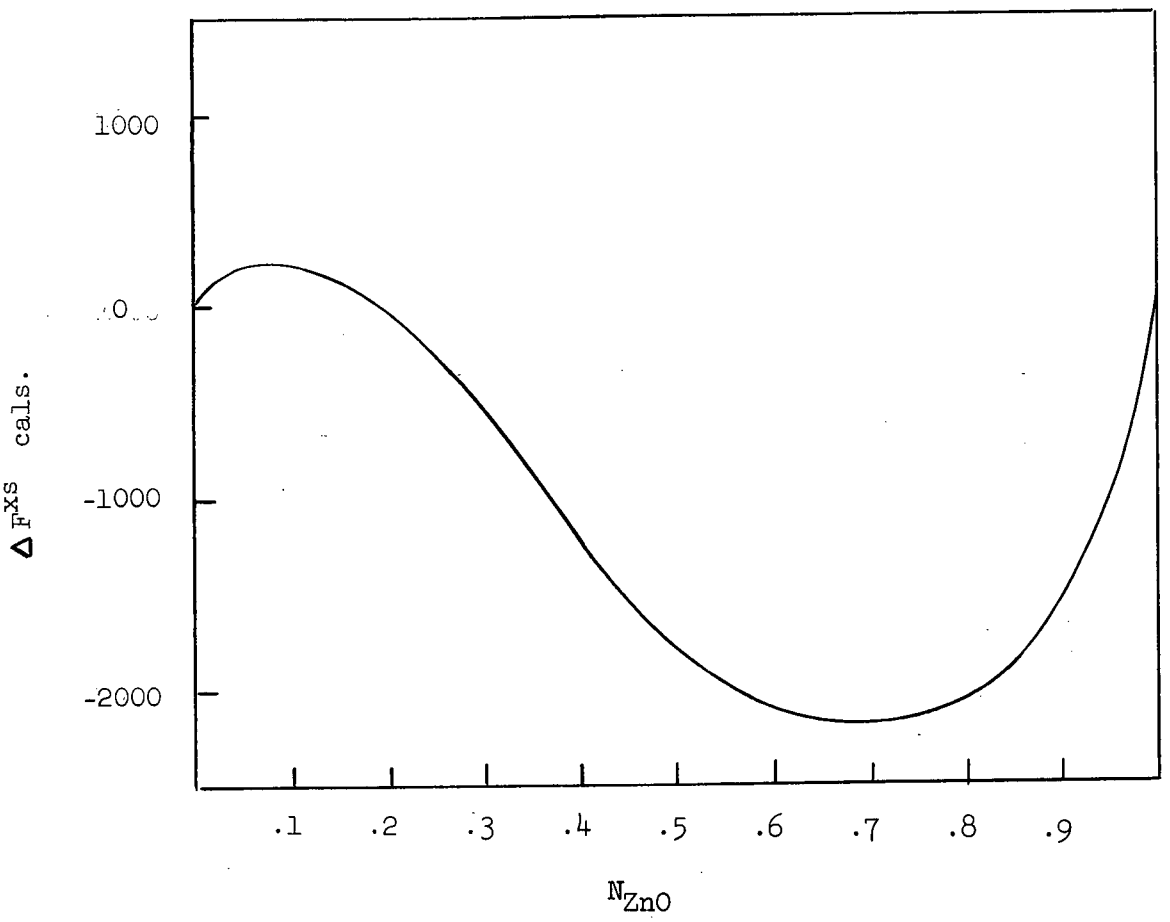

Figure 6. Calculated Excess Free Energy in the ZnO-SiO_2 Binary at 1600°C.

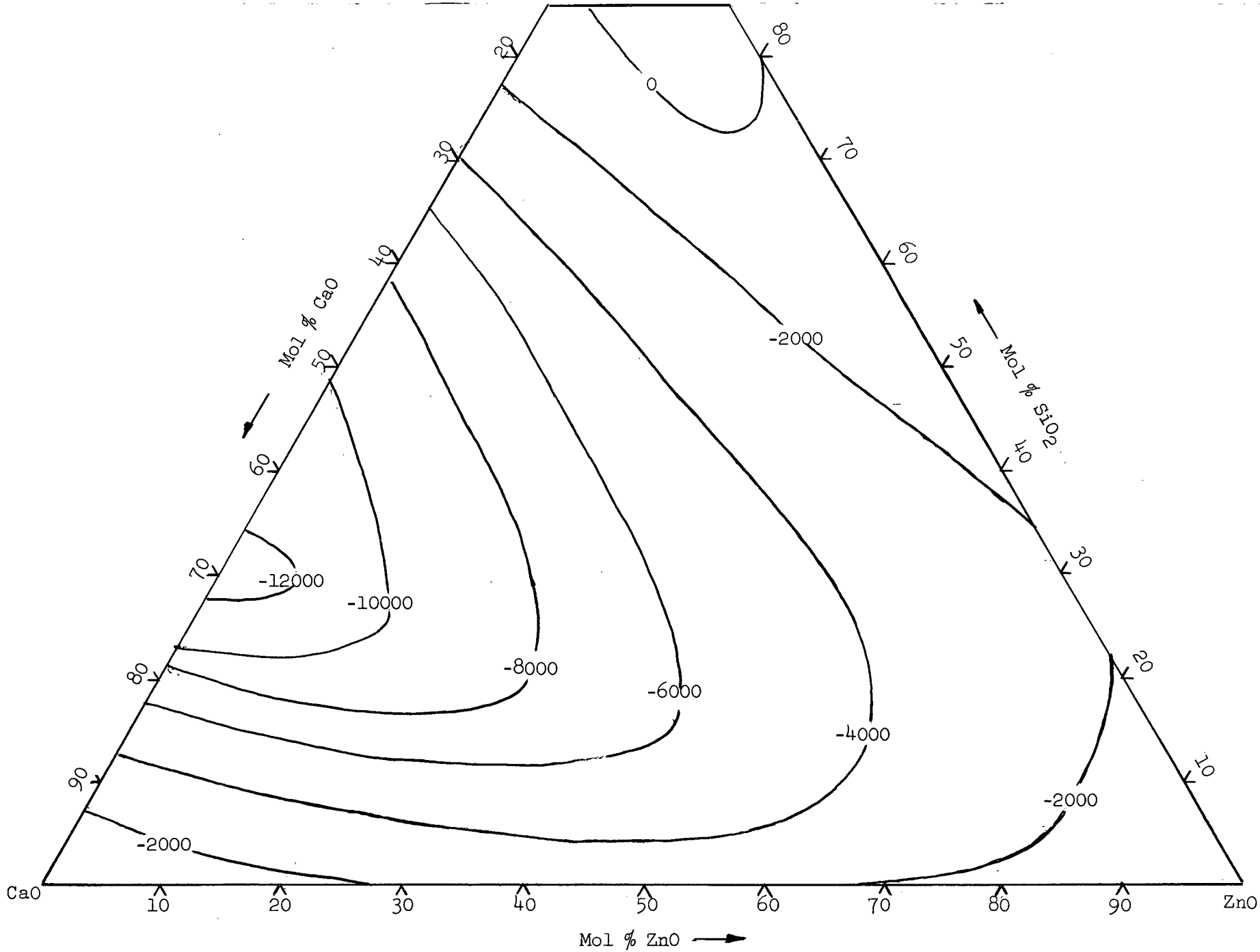

Figure 7. Calculated $\Delta \bar{F}^{xs}$ of the ZnO-CaO-SiO_2 Ternary at 1600°C

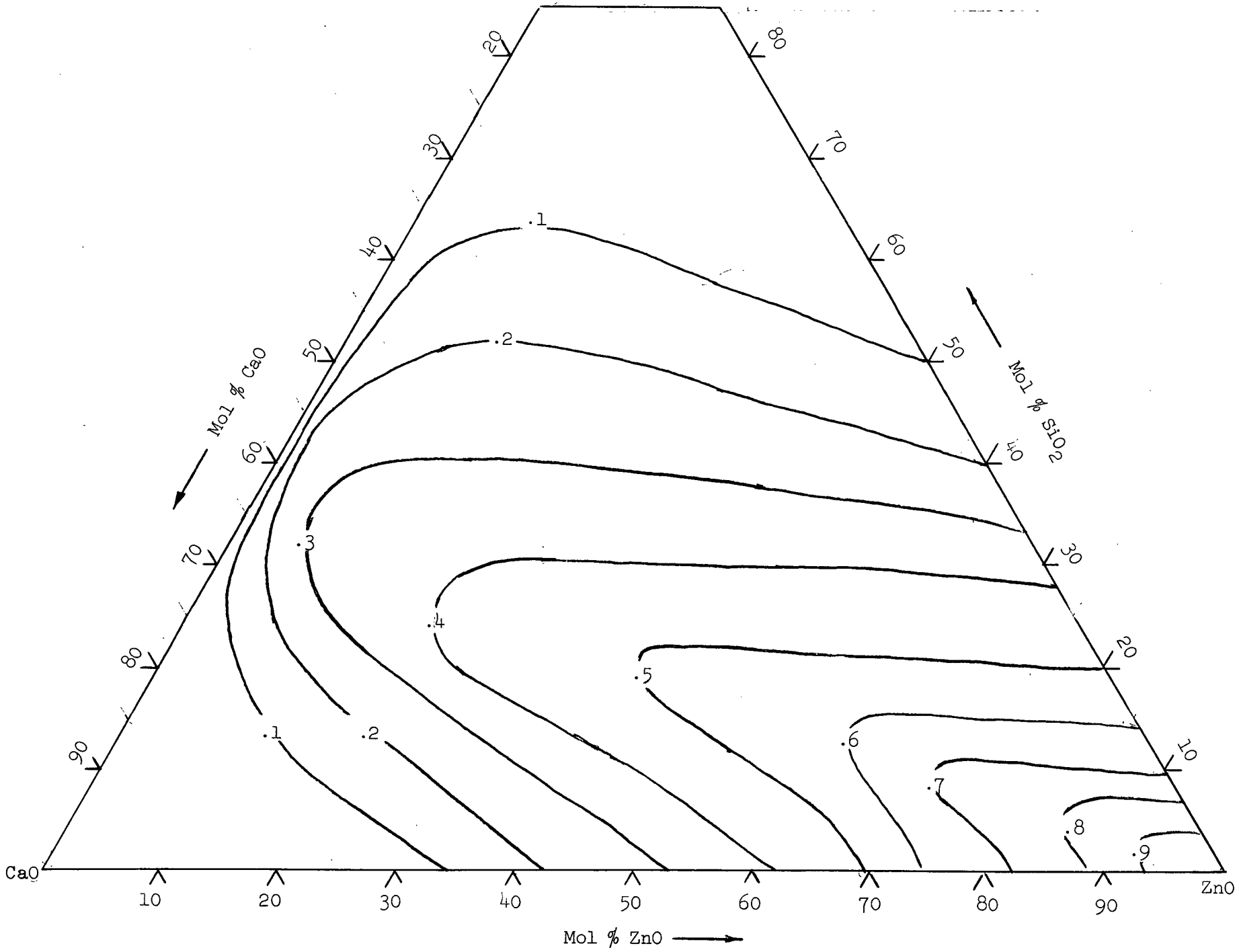

Figure 8. Calculated Isoactivity Lines for ZnO at 1600°C.

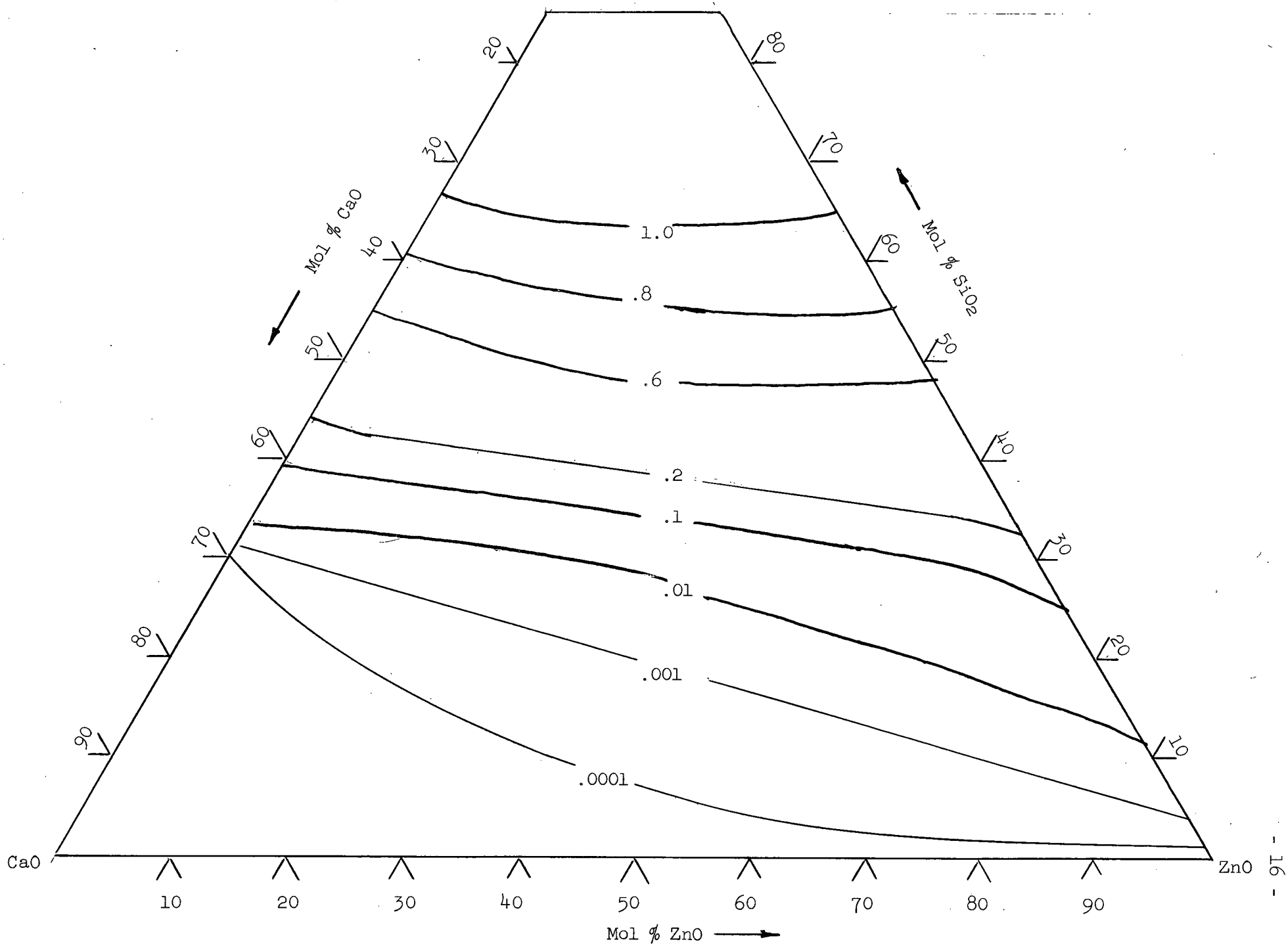

Figure 9. Calculated Isoactivity Lines for SiO_2 at 1600°C.

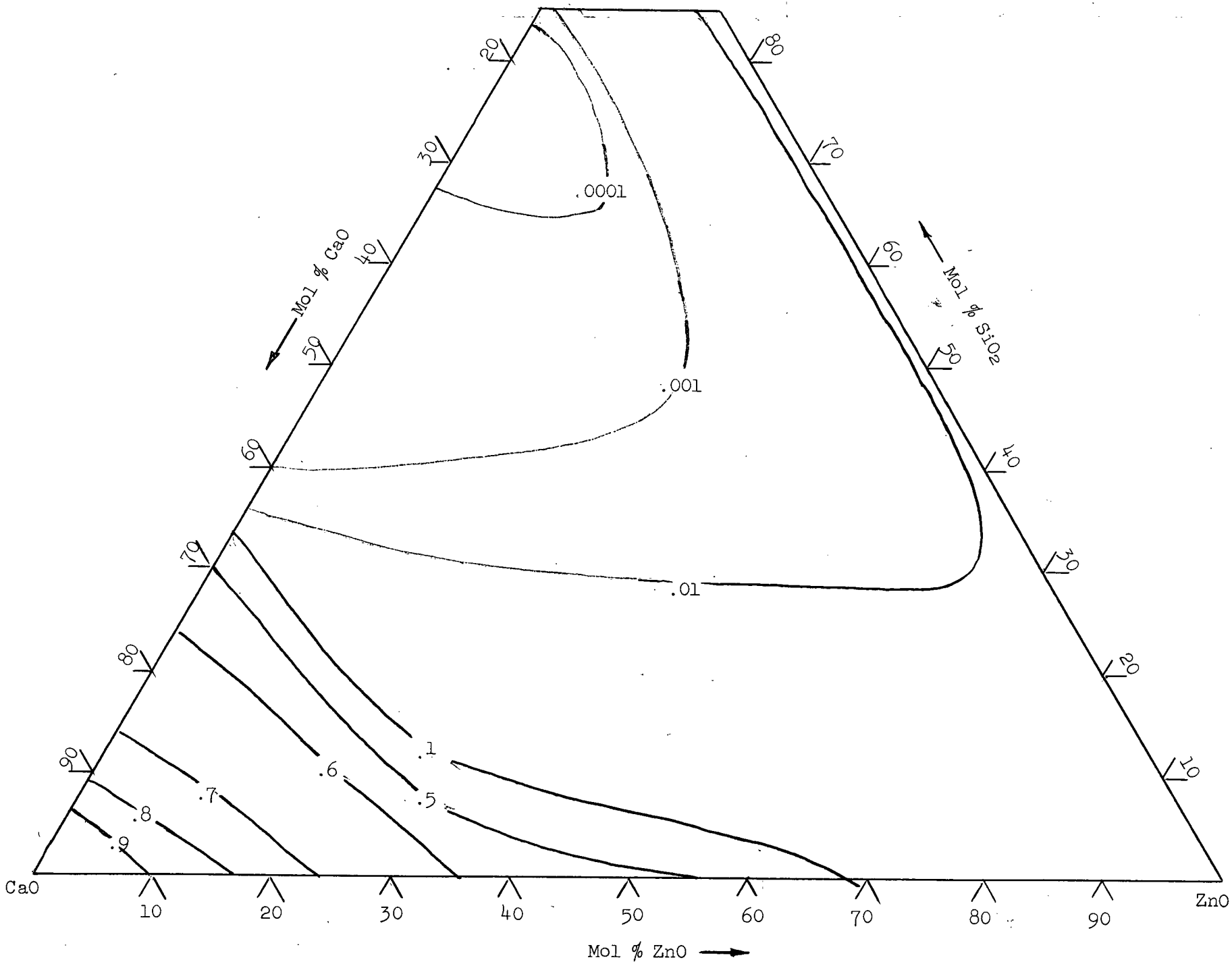

Figure 10. Calculated Isoactivity Lines for CaO at 1600°C.

EXPERIMENTAL

A Equipment

The experimental lay-out and apparatus are shown in figures 11 and 12.

1.) Oxygen Cell Design

A cell design similar to that of Fischer and Ackermann[22] employing air as the reference oxygen half cell was used (Figure 13). Such a design avoided any loading of the ceramic electrolyte and permitted its placement in the best position relative to the temperature gradient of the furnace. (Figure 14).

2.) Furnace

A vertical Super Kanthal furnace was used. It was capable of attaining 1600°C on a 1 3/4" diameter cross section about three inches in length. The power input at the experimental temperature (1300°C) was 1.9 kilowatts.

3.) Temperature Control

Furnace temperature was measured with a Pt-Pt-10% Rh thermocouple. Maximum sensitivity of control was achieved by setting the voltage at a known level for the temperature desired and having continuous power into the furnace. In this way it is estimated that furnace temperature and control were accurate to within $\pm$ 10°C. A Honeywell Brown Electronik controlling potentiometer was available and acted as a maximum temperature cut-off device.

4.) Emf Measurement

The oxygen cell emf was measured with a Pye portable potentiometer. It was found that this was as sensitive as a high impedance vacuum tube voltmeter. At 1300°C the emf could be measured to within $\pm$ 1 mv.

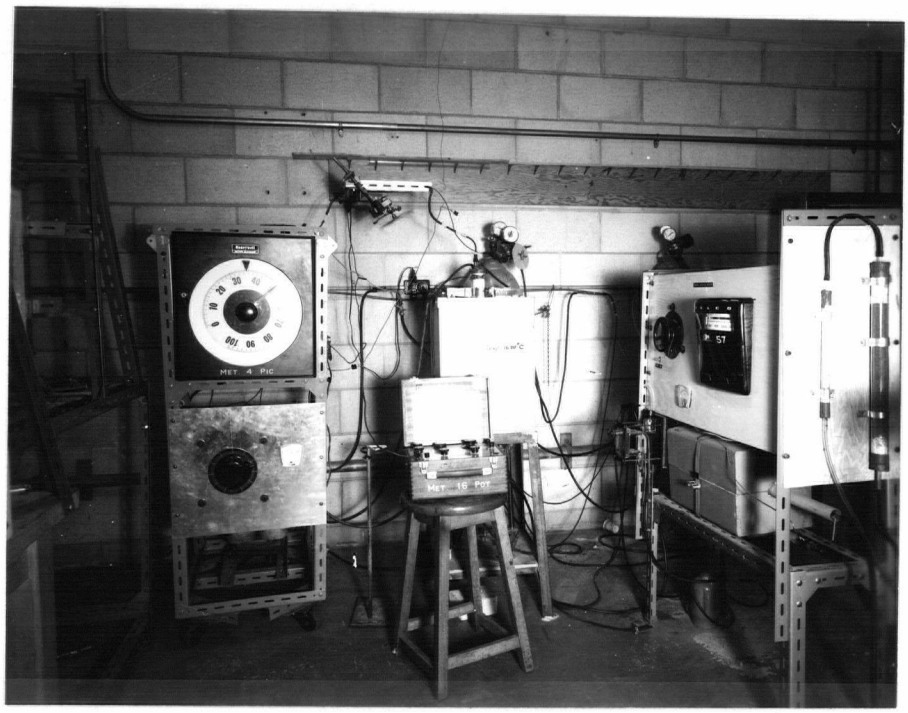

Figure 11. The Experimental Layout.

Legend

1. Brass End Cap-Water Cooled
2. O-Ring Seal
3. $0.85ZrO_2$-0.15CaO Impervious Tube (Solid Oxygen Electrolyte)
4. Pt-Pt 10%Rh Thermocouple
5. Inner Platinum Electrode
6. Outer Platinum Electrode
7. Crucible Containing melt
8. Mullite Furnace Tube
9. Fireclay Pedestal
10. Vitreosil Pedestal Rod
11. O-Ring Seal
12. Brass End Cap-Water Cooled
13. Anhydrite
14. Hot Copper Turnings
15. Silica Gel
16. Ascarite
17. Deoxo Catalyst
18. Silicone Oil Bubbler
19. Nitrogen Flow Meter
20. Needle Valve
21. Nitrogen Supply
22. Hydrogen Supply
23. Pye Potentiometer
24. Controller and Variac.
25. Air Supply

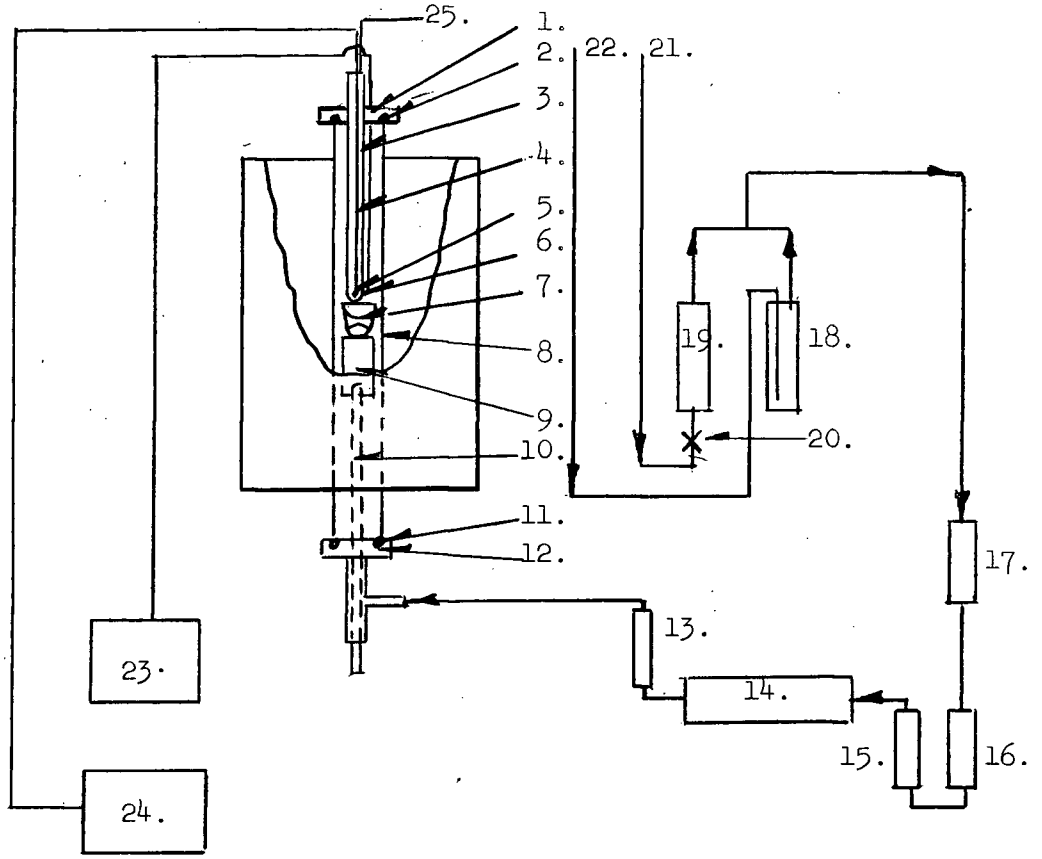

Figure 12. Schematic Diagram of the Experimental Apparatus

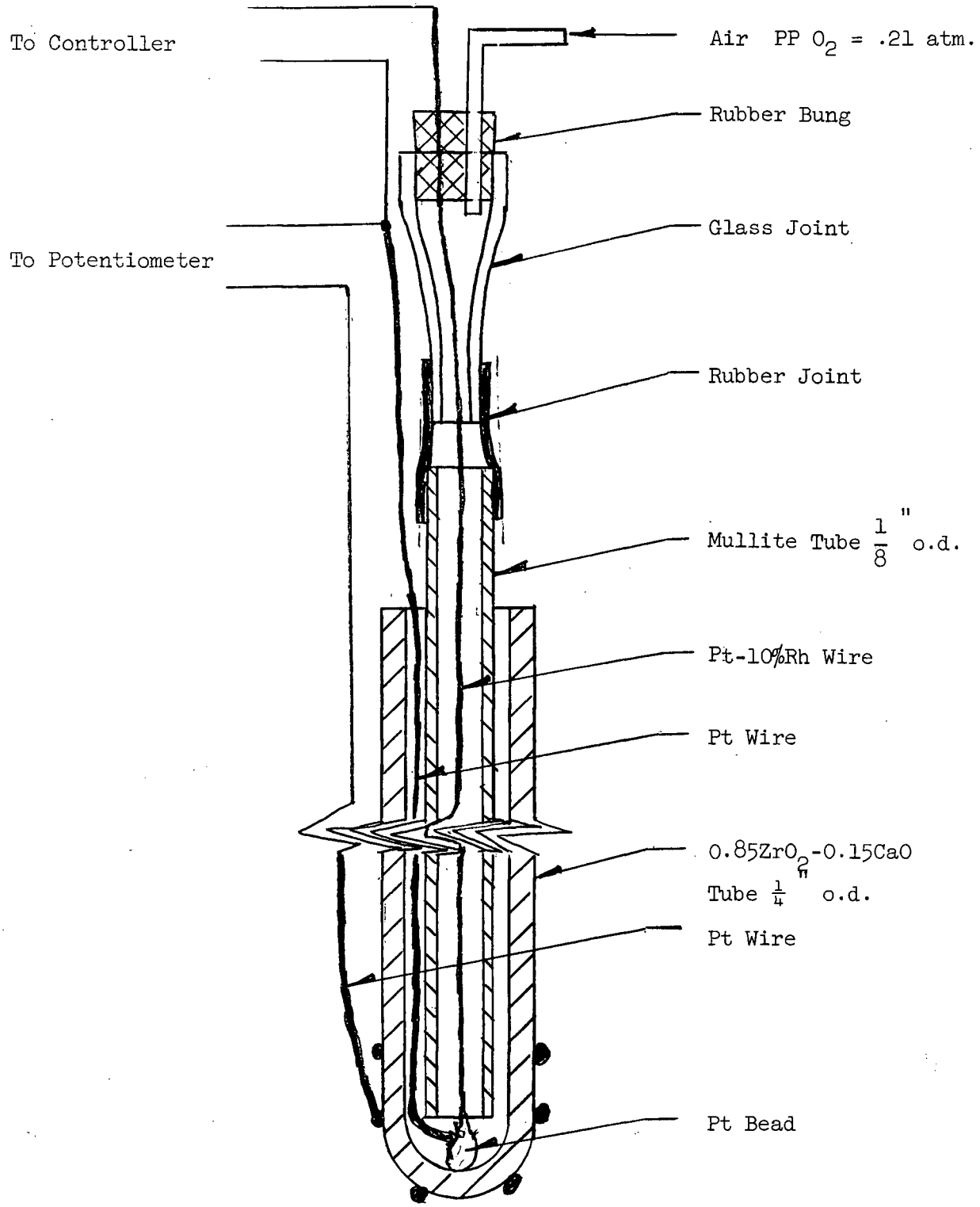

Figure 13. Oxygen Cell

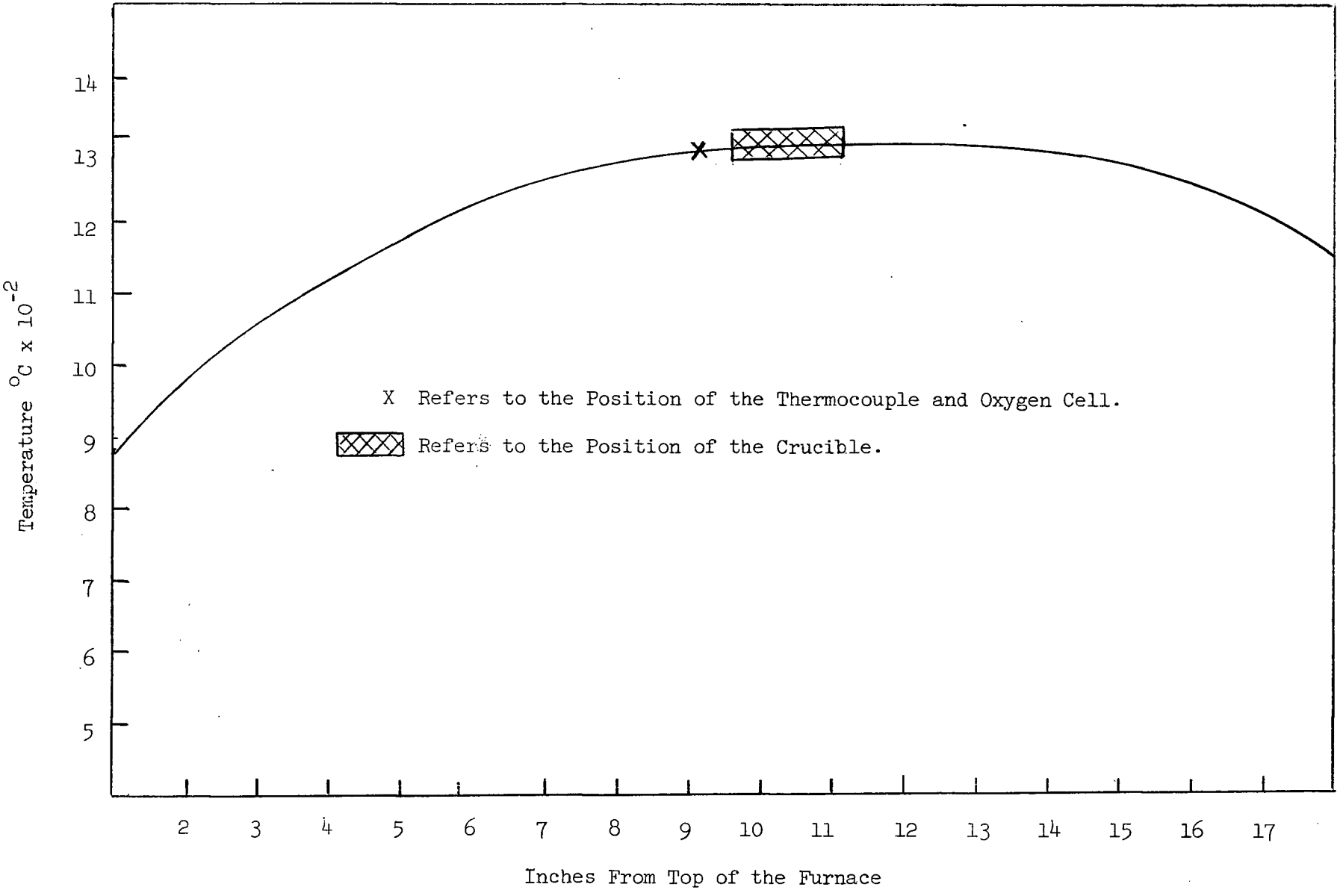

Figure 14. Temperature Profile of Super Kanthal Furnace at 1300°C.

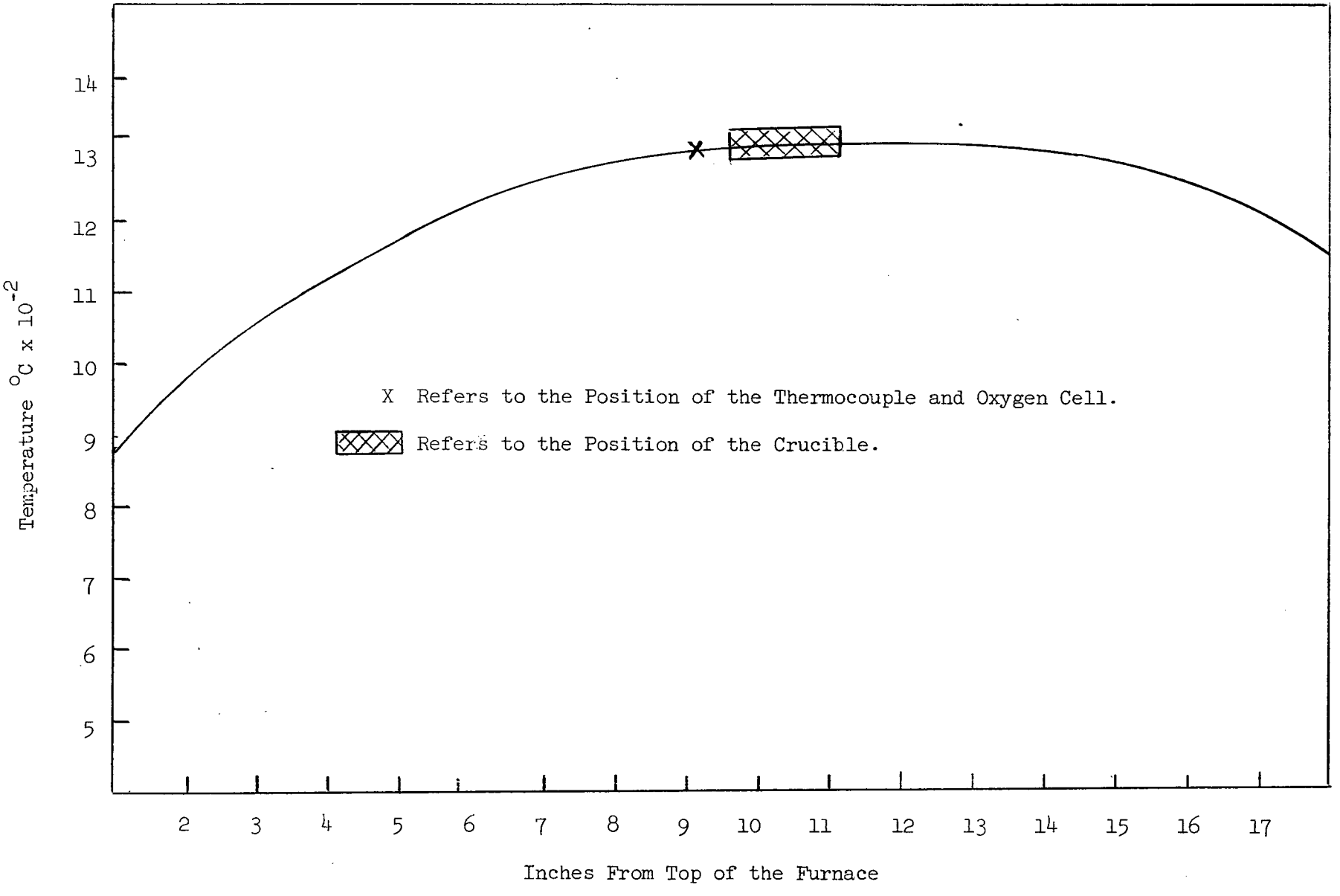

Figure 14. Temperature Profile of Super Kanthal Furnace at 1300°C.

5.) Purification Train

The gas purification train will be discussed under oxygen potential control in the section on procedure.

6.) Air Pump

It was found necessary to maintain a flow of air against the bottom of the cell to avoid the formation of an oxygen gradient from the top to the bottom of the cell. A small vibrator pump supplied sufficient air pressure to accomplish this.

B. Materials

1.) Reagents

Baker and Adamson analysed granulated zinc, shot copper, powdered zinc oxide and powdered calcium carbonate were used. Silica was standard commercial grade.

2.) Crucibles

Silica saturated slags were held in 20 ml. Vitreosil 97% silica crucibles. Non-silica saturated slags were contained in yttria stablized zirconia crucibles supplied by the Zircoa Corporation, 1 1/4" o.d. x 3" long.

3.) Oxygen Cells

The oxygen cells used were $0.85ZrO_2$ - 0.15CaO impervious tubes 1/4" od fifteen inches long, closed one end, supplied by Zircoa Corporation.

4.) Electrodes

The inner electrode was simply the platinum lead from the thermocouple held in electrical contact against the solid electrolyte by the thermocouple insulator. The outer electrode was a piece of platinum wire wrapped around the base of the cell immediately above the melt.

C. Procedure

A crucible containing about ten grams of alloy together with fifteen grams of slag was loaded into the bottom of the furnace, at a temperature such that the brass would remain solid. The system was purged with low oxygen potential gas. When a suitable emf was reached the pedestal was raised to bring the crucible just below the cell and the variac set to give the desired experimental temperature. The metal phase was sampled at various oxygen partial pressures allowing time for equilibrium to be established at each potential. When all the alloy was removed the furnace was cooled and the crucible withdrawn.

1.) Oxygen Potential

a.) Oxygen Potential Range Available

At any given temperature and zinc oxide activity two considerations fix the range of oxygen potential available. The lower side is determined principly by the boiling point of zinc in the alloy. At 1300°C with unit activity of zinc oxide this gives a lower oxygen potential limit of 2.0×10^{-10} atm. (Appendix IV). The highest oxygen partial pressure is fixed by the limit of detectability of zinc in the brass and by the necessity of keeping copper from oxidizing into the slag. Assuming that the oxidation of copper is the determining factor at 1300°C, the highest oxygen potential would be 1.1×10^{-4} atm. (Appendix IV).

b.) Oxygen Potential Control

The oxygen potential was controlled by the water equilibrium constant in a flow of commercial grade nitrogen into which a small amount of hydrogen was bled through a silicone oil bubbler. The oxygen potential was varied by adjusting the needle valve on the nitrogen flow meter to change the relative flow rates of the two gases. A total flow rate of about 100 cc's a minute was

sufficient to maintain equilibrium conditions in the furnace.

c.) Purification Train

The gas train consisted mainly of devices to help reduce the oxygen potential of the commercial grade nitrogen which probably contained about two percent oxygen. The deoxo catalyst served to combine most of the oxygen with hydrogen to form water. The hot copper turnings served as a further control as the oxygen potential of the gas should be determined by the equilibrium oxygen potential with solid copper at the temperature of the turnings. Ascarite was used to remove any CO_2 present and silica gel and anhydrite were used to reduce the water content of the gas.

d.) Duration of Run

The method of controlling oxygen potential was a large factor in the length of time a run was kept in the furnace. In order to keep the oxygen potential constant at any level it was necessary to continuously monitor the flow of the two gases. The longest run was eight hours.

2.) Zinc Activity

a.) Alloy Preparation

To reduce zinc loss it was felt inadvisable to simply load premixed metal powder into the furnace. Copper-rich brass ($N_{Zn} \simeq 0.01$) was prepared at the beginning of the experiment as none was readily available. Weighed amounts of the two metals were sealed in evacuated quartz and melted in the Super Kanthal furnace. The composition gradient of the alloy was slight and was no serious limitation.

b.) Sampling

The metal phase was sampled by inserting a 2 mm i.d. quartz quill into the melt and withdrawing a pencil of alloy with an attached aspirator bulb.

It was found that the introduction of the tube only momentarily lowered the oxygen potential and it returned to its original value within a minute of withdrawal.

c.) Analysis

Metal specimens were dissolved in diluted 1:1 nitric acid and the solution analyzed for zinc using a Unicam SP-90 atomic adsorption spectrophotometer. For pure zinc the effective sensitivity limit of this instrument was found to be about 0.05 µg/ml of solution. For a 0.1 gram sample dissolved in the minimum amount of nitric acid and made up to 10 ml., the minimum detectable zinc is about 0.005 mol percent. Pure copper has some absorption at the 2139A° line used for zinc analysis. One gram of copper in fifty cubic centimeters of solution gives an absorption equivalent to one microgram per millilite of zinc. This coincides with the sensitivity of the instrument for pure zinc. Hence the effective sensitivity of the instrument for detecting zinc in a copper rich brass is 0.01 mol percent. In all the specimens the experimental ratio was in the order of one hundred parts of copper to one part of zinc. In this range the exact proportion interfered little (Figure 18). A brass standard containing one hundred parts of copper to one part of zinc was used in all the analysis. Accuracy was estimated at $\pm$ 5%.

3.) Slags

a.) Preparation

On initial runs it was found that there was considerable difficulty in melting the oxide powders to form a slag during a run at temperatures only slightly higher than the estimated melting point of the slag. Segnit and Wolfe's[23] technique for quenching prefused slags in a platinum crucible was adapted for use in the Super Kanthal furnace. The furnace design was not very suitable for this work since a crucible had to be lowered on the pedestal and the pedestal removed before the crucible could fall into a bucket of cold water under the furnace. Thus higher melting point slags could not be readily made. Mainly

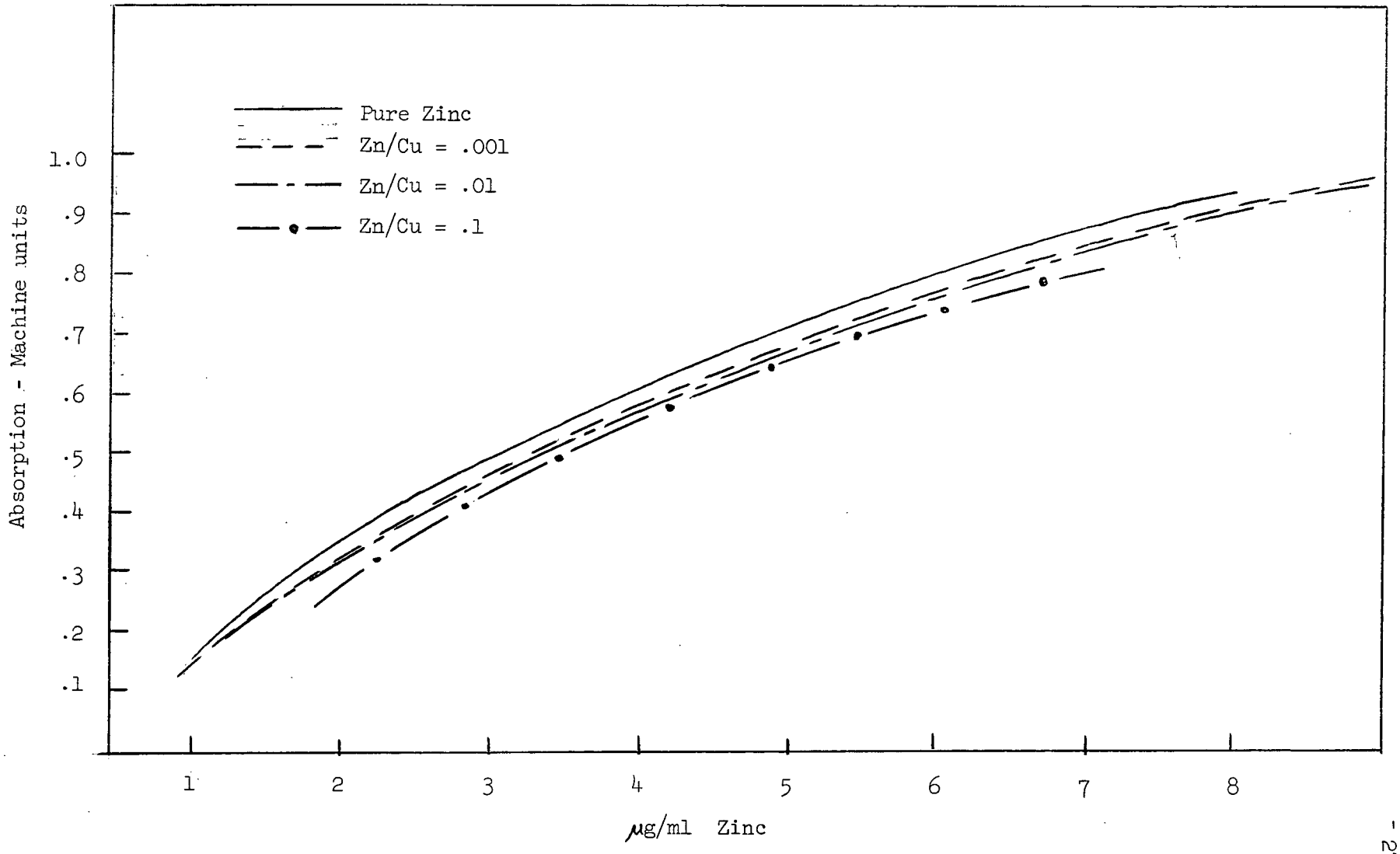

Figure 15. Standardization Curves for the SP-90 Atomic Absorption Unit as a Function of Zn to Cu ratio in the Standards.

for this reason it was decided to work principly along the 1300°C silica saturation line. In addition the job of chipping only partially glassy slags from the platinum crucible was somewhat laborious.

b.) Sampling

Slags were sampled by a cold steel rod with a notch cut into the lower end.

c.) Analysis

Slag samples of about 0.5 gram were ground to minus 100 mesh and treated with a mixture of equal parts of concentrated hydrofluoric and perchloric acids in a platinum crucible. The baked constant weight residue was weighed as metal chlorides. The difference was assumed to be silica. The residue was treated with boiling water to bring the chlorides into solution. The solution was then analyzed for zinc and copper using the absorption spectrophotometer. The difference was again used to check the original CaO to SiO_2 ratio of the oxide powders.

4.) Time for Equilibria

The length of time required for equilibrium to be established was arbitrarily set at one half hour to minimize the length of time during which the gas flows would require continuous monitoring. In figure 16 a plot is given from one run of the actual over the average ZnO activity as a function of time. It is seen that although there is considerable scatter, the length of time between readings had little effect between one half hour and four hours. It was assumed that equilibrium was attained within one half hour at each different level of oxygen potential.

5.) Reversibility of the Oxygen Half Cell

The most important condition for oxygen cell reversibility is that the transference number for oxygen ions be unity. As a further check that the cell

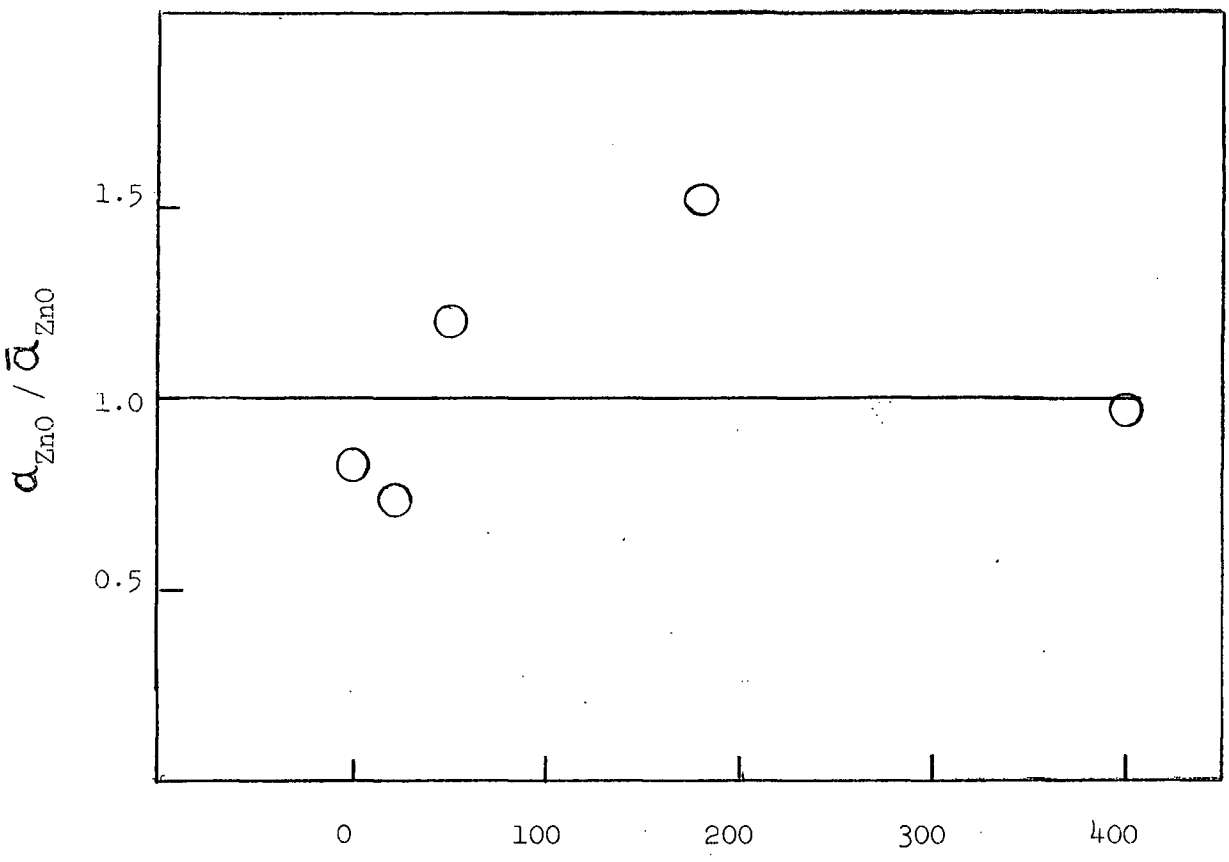

Figure 16. Experimental Variation in Activity of ZnO as a Function of Time.

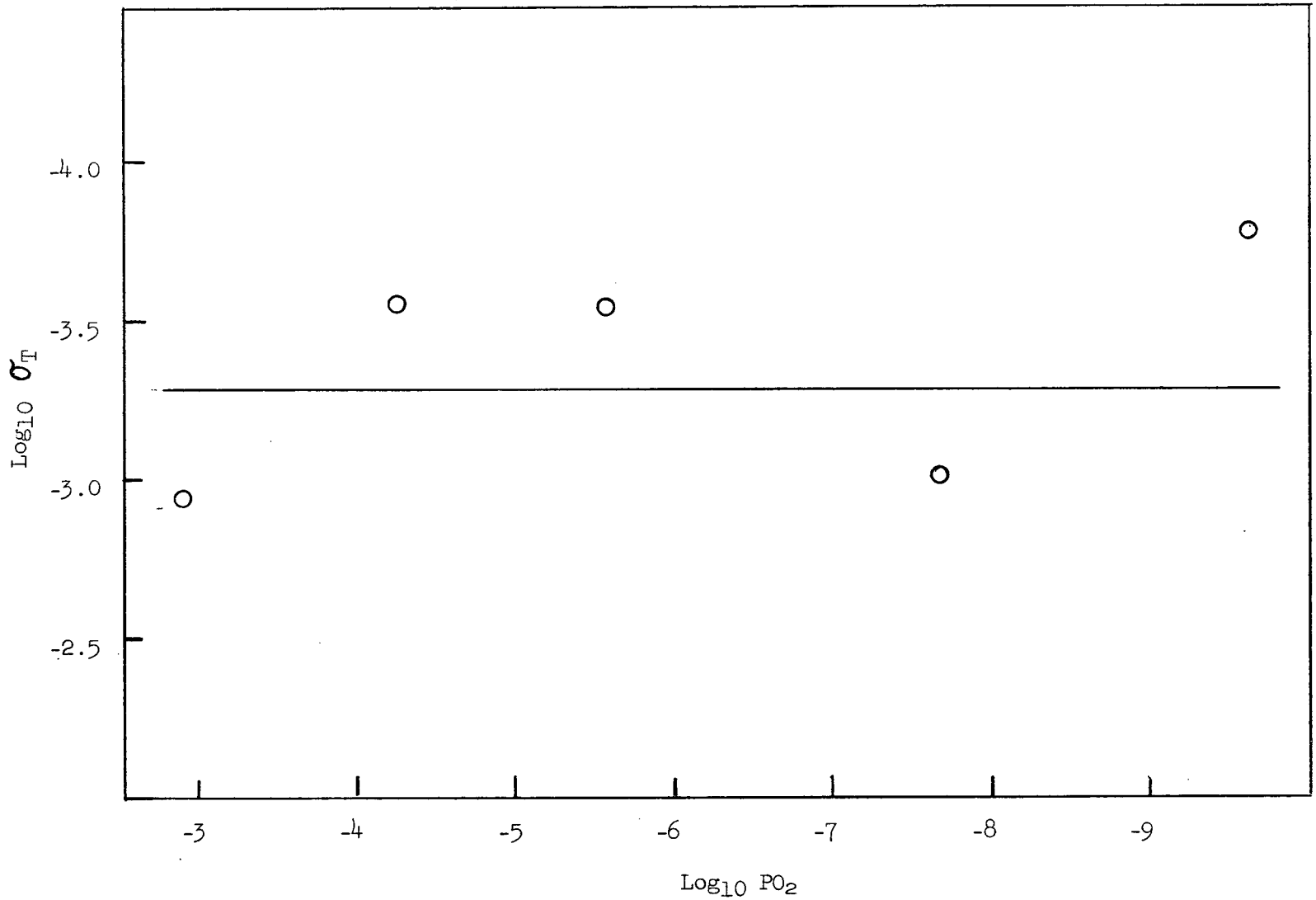

Figure 17. Conductity of 0.85 ZrO_2-0.15 CaO Solid Electrolyte as a Function of Oxygen Potential at 1300°C.

was measuring the true oxygen potential of the system two brief experiments were carried out. Using a Pye potentiometer as a voltage source it was found that after imposing a one volt emf across the cell in either direction, the resting potential of the operating cell was unchanged. Thus it was concluded that the cell was not polarized. A simple ohmmeter was used as a conductivity meter at several different values of oxygen partial pressure. It is seen (Figure 17) that the variations in conductivity is slight over a relatively wide range of oxygen partial pressure. This indicates that oxygen ions are the major charge carriers.

RESULTS

A. Zinc Oxide Activity

The experimental results are presented in table 1. The activities of zinc oxide with respect to the solid standard state are measured at the particular experimental temperature using the free energy expression given by Wicks and Block[9].

Reproducibility is well within the calculated standard deviations which are admittedly quite large. Considering that this work required a three phase equilibrium at high temperature it is not unreasonable to find such large standard deviations.

Table I

Experimental Zinc Oxide Activities

KEY	TEMP °C	a_{Zn}	EMF mv	PPO_2 x10^8	$a_{Zn}PPO_2^{\frac{1}{2}}$ x10^7	a_{ZnO}	$\bar{a}_{ZnO}$	SLAG ZnO	SLAG CaO	SLAG SiO_2	$\sigma/\bar{a}_{ZnO}$
D1	1240	.00155	490	4.2	3.17	1.48					
D3	1240	.00083	524	1.18	.897	.44	.94	26.5	23	50.5	.48
D4	1235	.00072	483	4.4	1.51	.75					
E1	1310	.00189	490	8.37	5.45	.733					
E2	1300	.00096	507	4.71	2.1	.283					
E3	1305	.00086	472	13.3	3.14	.422	.45	24	21	55	.38
E4	1305	.00057	455	22	2.67	.36					
F1	1305	.0015	536	1.88	2.05	.275					
F2	1305	.00129	494	6.96	3.4	.457					
F3	1320	.00154	499	7.54	4.19	.538	.519	24	21	55	.23
F4A	1320	.00141	494	8.37	4.07	.523					
F4B	1320	.00189	494	8.37	5.45	.70					
F6	1315	.00373	554	1.68	4.82	.620					
G1A	1340	.00523	708	.021	.755	.364					
G1B	1340	.00555	708	.021	.802						
G2	1335	.00501	653	.094	1.54	.755	.503	24	21	55	.36
G3	1320	.00328	573	.835	3.0	.39					

KEY	TEMP °C	a_{Zn}	EMF mv	PPO_2 x10^8	$a_{Zn}PPO_2^{\frac{1}{2}}$ x10^7	a_{ZnO}	$\bar{a}_{ZnO}$	SLAG ZnO	SLAG CaO	SLAG SiO_2	$\sigma/\bar{a}$
I1	1365	.0019	409	149.	23.1	1.21					
I2	1365	.0022	383	348.	41.	2.15	1.11	42	22	36	.62
I3	1365	.0017	475	22.	.79	.42					
I4	1365	.0030	475	22.	1.4	.735					
J1	1330	.00345	501	8.36	9.93	.827					
J2A	1325	.00238	480	1.38	8.85	.737					
J2B	1325	.00225	480	1.38	9.25	.772	1.00	42	22	36	.28
J3	1330	.0028	460	2.65	14.4	1.2					
J4	1330	.0039	463	2.2	18.3	1.52					
J6	1345	.003	484	1.49	11.6	.97					
K1	1335	.0032	600	1.01	3.2	.263					
K2	1365	.00305	477	24.	1.48	.78	.405	14	27.5	58.5	.13
K3	1345	.0033	429	80.	2.95	.209					
K4	1345	.0012	480	18.7	5.2	.37					

B. Solid Zinc Oxide Saturation Line

($a_{ZnO} = 1$)

In figure 18 the results of two separate runs are plotted using a slag saturated in both zinc oxide and zinc orthosilicate (.22 CuO, .42 ZnO, .36 SiO_2). It is seen that the line calculated from the assumption that zinc oxide activity is unity (i.e. $a_{Zn} \times PPO_2^{1/2} = K_{eq.}$ w.r.t. solid ZnO) fits these points reasonably well. Hence it is concluded that at 1300°C the transport number for oxygen ions in the solid electrolyte 0.85 ZrO_2 - 0.15 CaO over an oxygen potential range of 2.3×10^{-6} to 8.4×10^{-8} is unity.

C. Slag Analysis

Extensive slag analysis was done on one of the early runs and showed that the variation in composition of the slag over a six hour period was within five percent of the original fraction of oxide powders. This was negligible in comparison with the variation in measured ZnO activity and hence it was assumed for the other runs that the slag composition present was that given by the original oxide mixture.

The presence of large amounts of cuprous oxide in the slag was evident from those runs in which the controlled atmosphere was lost and copper was allowed to oxidize. These slags were very dark brown in colour and textured rather than glassy. In the analyzed slag samples which were clear or slightly green in colour the maximum cuprous oxide content was less than one mole percent. As long as the slag remained clear it was assumed that the amount of cuprous oxide present was negligible.

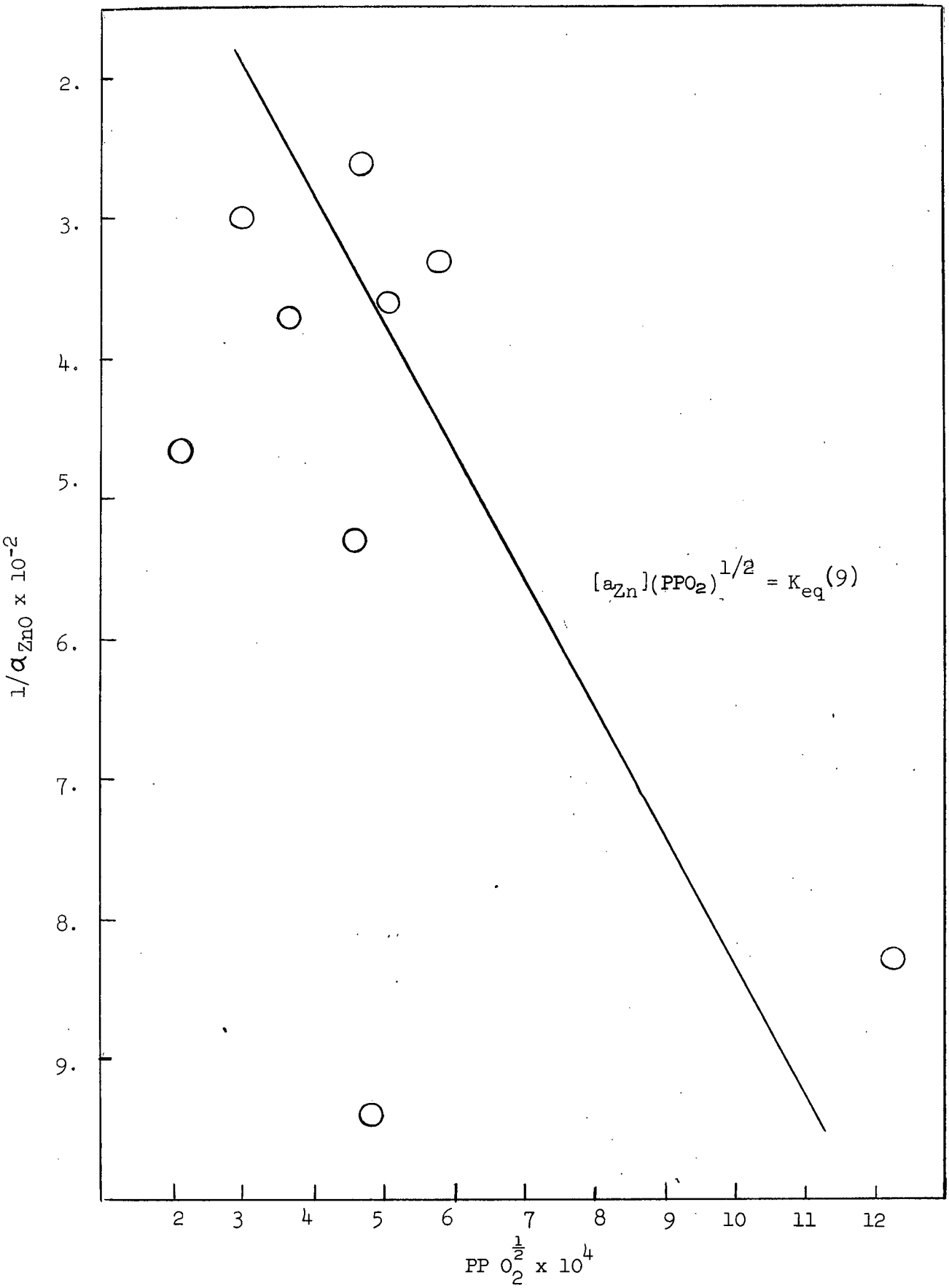

Figure 18. Data for Runs I and J (ZnO Saturated) Together with Calculated Theoretical Line for Zinc Oxide Saturation.

INTERPRETATION OF RESULTS

A. Calculation of a ZnO (Liquid Standard State) in $ZnO-CaO-SiO_2$ Slags

In order to compare the experimental results with those calculated by Toop's[16] method at 1600°C it is necessary to recalculate these activities using the pure metastable liquid as the standard state. The entropy of fusion for zinc oxide (6 E.U.) established from thermodynamic data (Appendix II) was used together with the regular solutions theory temperature adjustment. These results are given in table 2.

Table II

Activity of ZnO with respect to Metastable pure liquid ZnO at 1600°C

Run	$\bar{a}_{(s)}$	$a_{(l)T}$	γ_T	$\ln\gamma$	$\gamma_{1600°C}$	$a_{(l)\,1600°C}$
D	.94	.21	.792	-.233	.828	.22
E	.45	.124	.515	-.662	.571	.14
F	.534	.15	.623	-.472	.669	.16
G	.503	.15	.623	-.472	.669	.16
I	1.11	.35	.833	-.182	.853	.36
J	1.00	.29	.691	-.368	.729	.31
K	.405	.12	.857	-.154	.875	.12

B. Comparison between Experimental a_{ZnO} and Calculated ZnO Isoactivity Lines in the ZnO-CaO-SiO_2 System

The activities from Table 2 are plotted in Figure 19 together with the zinc oxide isoactivity lines at 1600°C from section III. The two points along the silica saturation line at 1300°C check the upper shape of the line $a_{ZnO} = 0.1$. The slag in equilibrium with solid ZnO and Zn_2SiO_4 at 1300°C gives an activity very close to the calculated activity at that point. Insufficient work was done to validate this theoretical treatment but the slags studied produced several activities remarkably close to those calculated from binary data by Toop's method[16]. It should be remarked that these ZnO activities were actually measured with reference to solid zinc oxide at 1300°C. It is assumed that the regular solution theory temperature adjustment is valid and that the entropy of fusion of ZnO is 6 E.U. in the calculations comparing these activities with the calculated isoactivity lines in Figure 12.

C. Comparison with Davenport's Calculated a_{ZnO} Data for the ZnO-CaO-SiO_2 Ternary

It is difficult to make comparisons between this work and work done previous to Davenport. All these studies measured ZnO activities in slags containing a large percentage of FeO in contact with Fe. The presence of this FeO tends to complicate the effect of the increasing CaO to SiO_2 ratio on the activity of ZnO.

The agreement between this work and Davenport's calculated data is rather poor (Figure 20). Several reasons may be given by way of explanation. The entropy of fusion for zinc oxide used in the present study was 6 E.U. Davenport estimated a value of 2.85 E.U.[5]. The excess free energy of the Zn-Cu system was found to have the following temperature dependence

$$\overline{\Delta F}^{xs}_{Zn} = -8200 + 2.58T$$

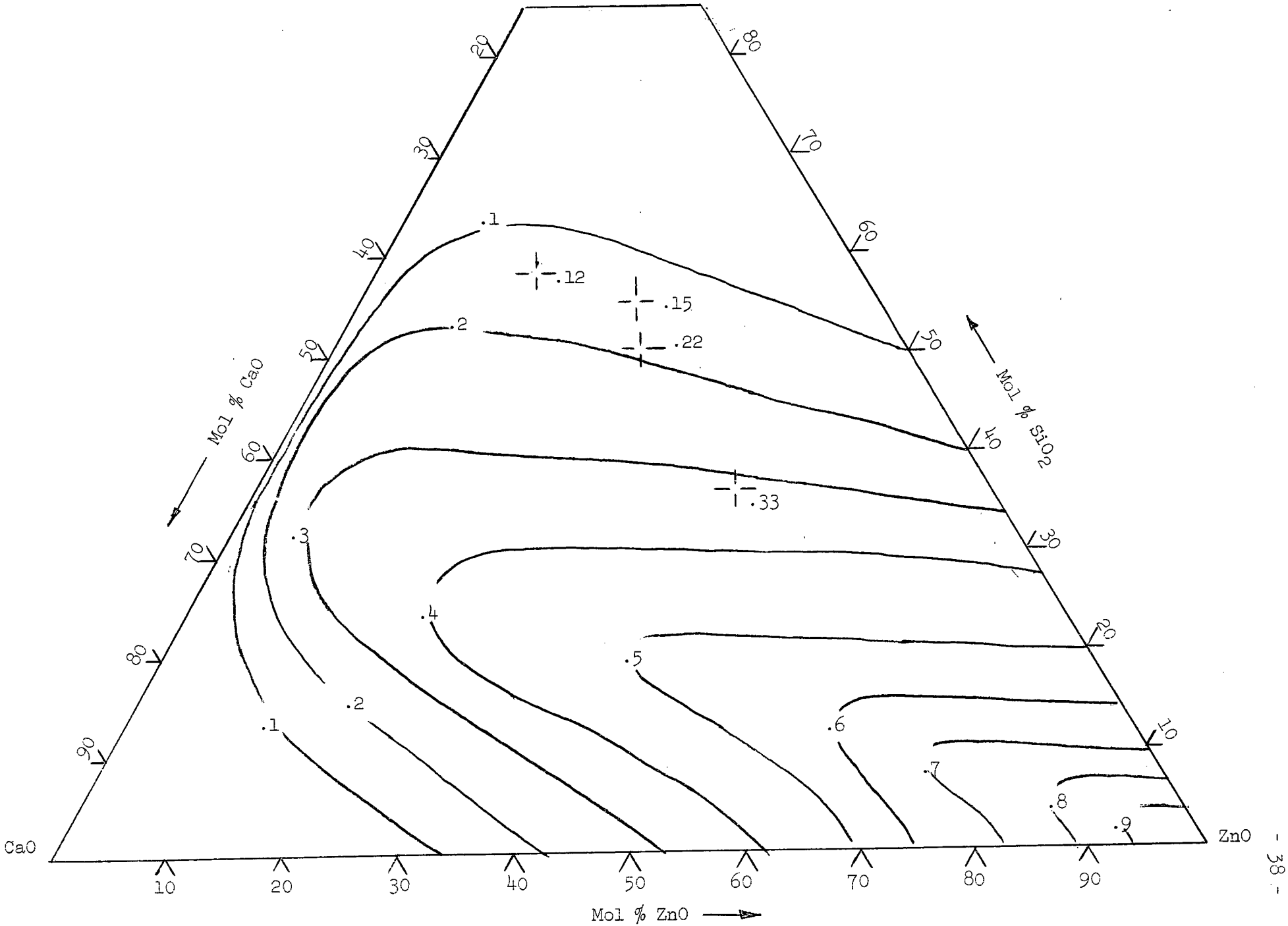

Figure 19. Measured ZnO Activity Values Compared with the Calculated ZnO Isoactivity Lines in the ZnO-CaO-SiO_2 Ternary.

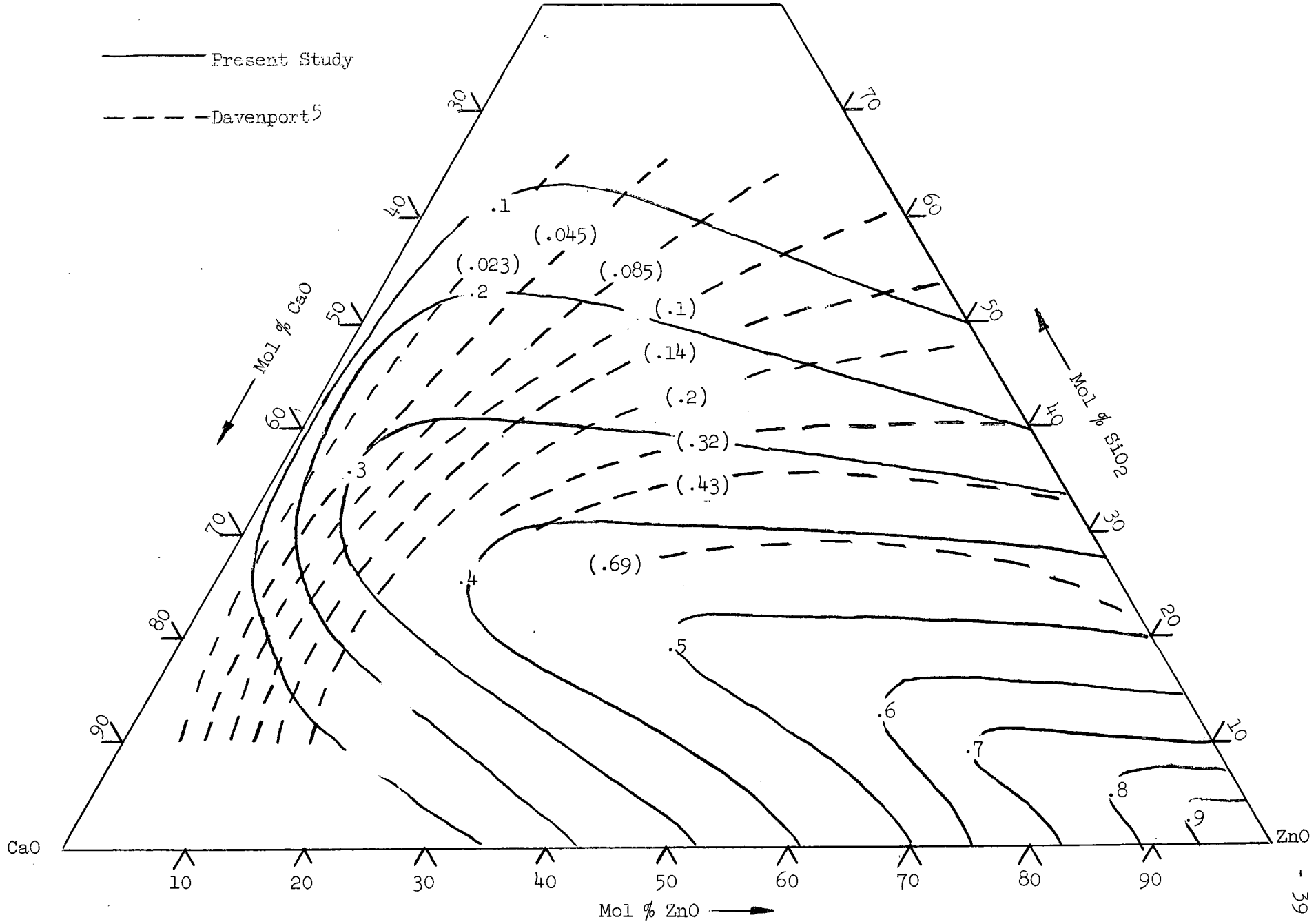

Figure 20. Comparison Between the Isoactivity Lines for ZnO at 1600°C Calculated by Davenport[5] and in the Present Study.

at low zinc composition. Davenport assumed complete regularity with an interaction energy of 7550 cals mol^{-1},[5]. Different methods of combining the auxiliary data were used in the two investigations. The present study used Toop's ternary integration technique based on the regular solution theory; Davenport used Schumann's ternary integration[24] and tangent intercept techniques[25] Both are based on the Gibbs Duhem relationship and hence should be compatible. It is quite obvious that the two studies measured activities in slags of widely different composition and it may well be that a slightly different theoretical treatment might bring both closer into agreement.

D. Comparison with Work by Azuma, Goto and Ogawa[6]

In keeping with their results it is seen that an increase in lime content to move the slag composition away from the line of silica saturation increases the activity coefficient of zinc oxide in the slag.

E. Comparison Between ZnO-CaO-SiO_2 and FeO-CaO-SiO_2 Ternaries

1.) ZnO-SiO_2 and FeO-SiO_2 Binaries

In figure 21 the excess free energy of the ZnO-SiO_2 binary is replotted together with Elliott's curve for the excess free energy of FeO-SiO_2[7]. The seemingly large difference between the two curves is attributed to the fact that the FeO-SiO_2 binary has slight positive deviation from ideality whereas the ZnO-SiO_2 binary has slightly greater negative deviation. The difference between them is never much greater than two kilocalories. When based on the solid standard states both curves are relatively close to ideal[8].

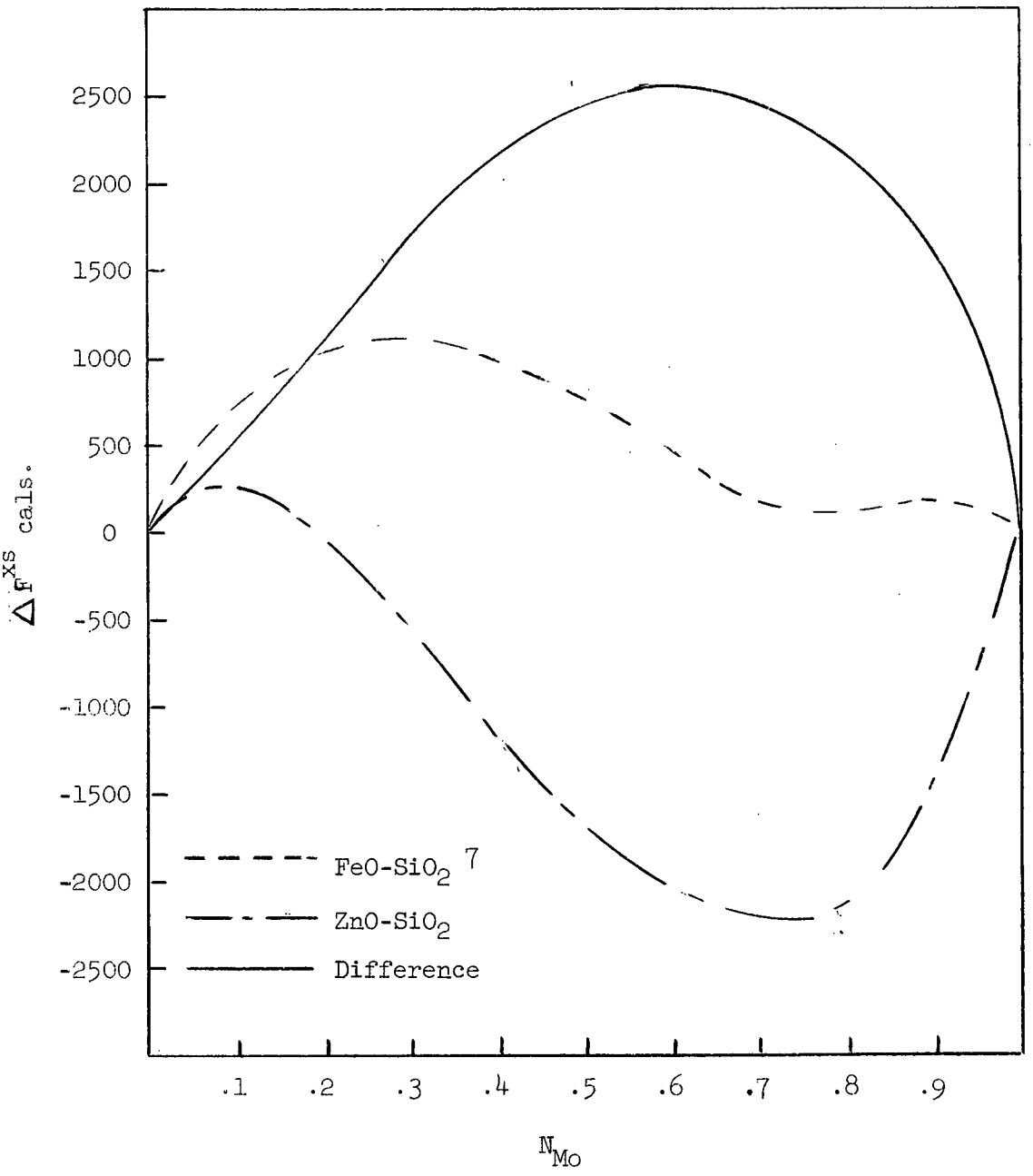

Figure 21. Comparison Between the Excess Free Energies of the Binaries FeO-SiO_2 and ZnO-SiO_2 at 1600°C.

2.) FeO-CaO-SiO_2 Ternary

The excess free energy contours and the isoactivity lines for FeO are shown in figures 22 and 23 respectively. Figure 22 shows a somewhat larger area with a positive excess free energy than does the corresponding figure for zinc oxide (Figure 7), but otherwise the shape of the contours is quite similar over most of the diagram. The isoactivity lines for FeO have a characteristic projection extending further towards the lime orthosilicate composition than does the characteristic projection for the zinc oxide isoactivity lines (Figure 8). This is in keeping with the slightly more basic behaviour of ferrous oxide.

SUGGESTIONS FOR FURTHER WORK

The most important limitation was the effective restriction on slag melting point because of the technique used for slag preparation. If an induction furnace had been available, slags could have been prefused in air using a platinum crucible as a susceptor. The crucible could then have been immediately quenched in water on removal from the coils.

At 1600 °C, for unit activity of zinc oxide:

$$[Zn](PO_2)^{\frac{1}{2}} = 8.7 \times 10^{-5} \quad (9) \qquad \ldots(9)$$

At this temperature the zinc-copper alloy boils at a zinc activity of approximately 0.01 (Appendix IV). From the thermodynamics of the copper-oxygen equilibrium, this will result in an activity of about 0.2 for cuprous oxide in the slag, which is no longer negligible.

Further work might be done using a modification of the technique used by Richards and Thorne[4]. Using a horizontal bed furnace, it would

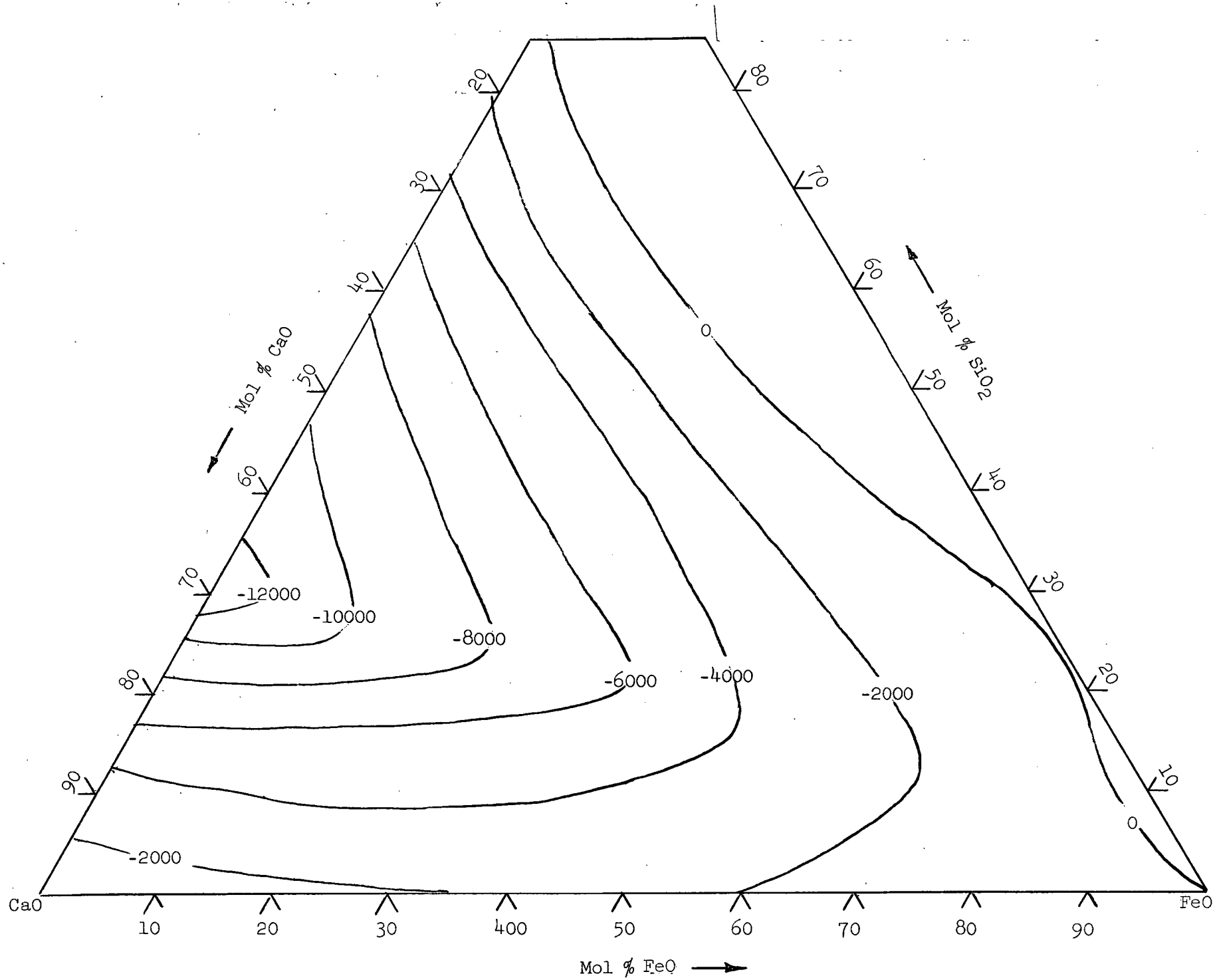

Figure 22. Calculated ΔF^{xs} of the FeO-CaO-SiO_2 Ternary at 1600°C.

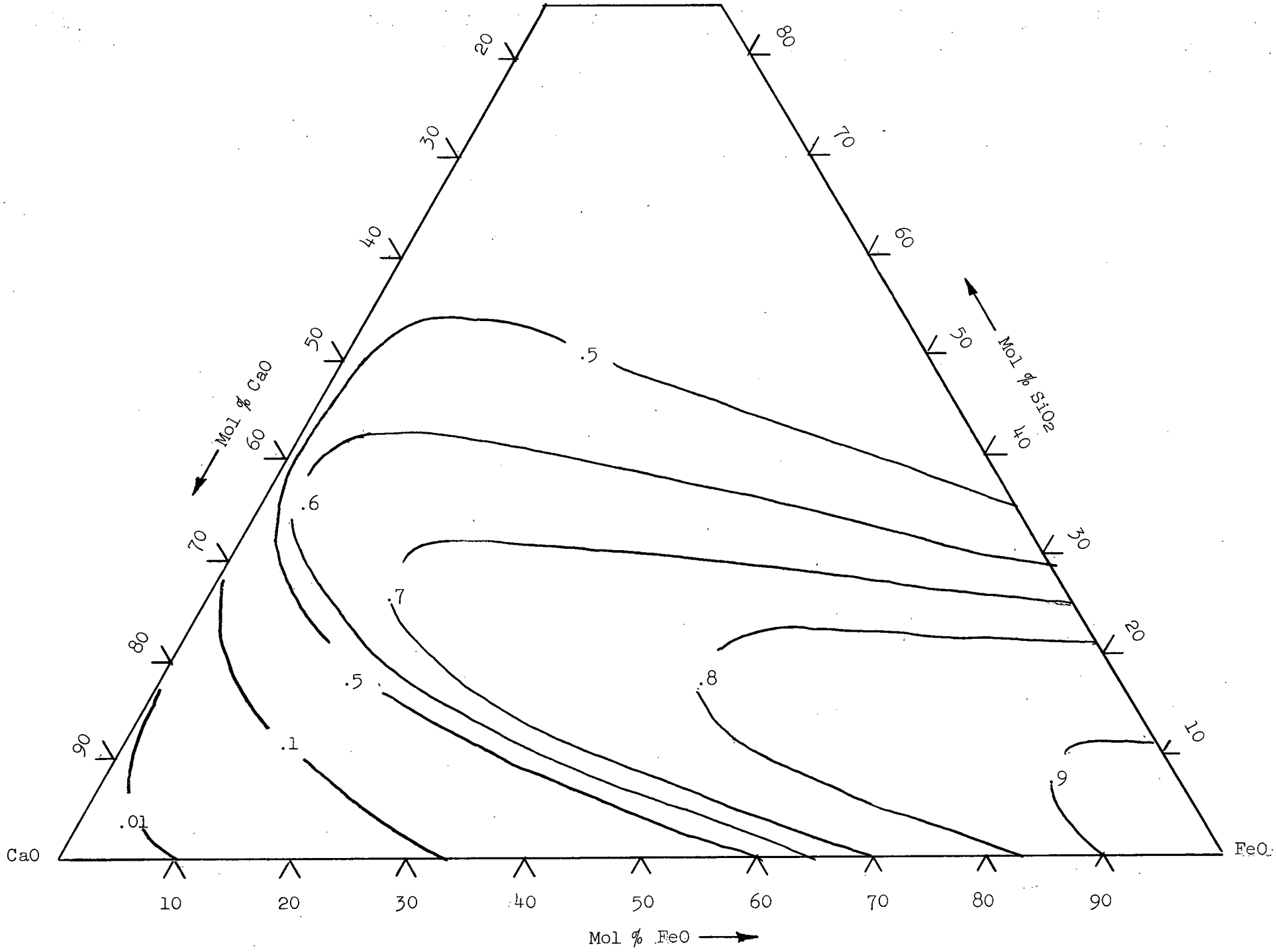

Figure 23. Calculated Isoactivity Lines for FeO at 1600°C.

be relatively simple to use a zinc source to establish a zinc partial pressure in the incoming low oxygen potential gas. Slag zinc loss would be completely avoided. Slags could be equilibrated with this gas in a platinum boat, circumventing the problem of containment for a slag-metal equilibrum melt. Zinc activity could then be determined by measuring the zinc partial pressure of the equilibrium gas. The oxygen potential could be measured using an oxygen half-cell as in the present study. The slag could be sampled once equilibrium conditions were established.

CONCLUSIONS

Activities of ZnO in $ZnO-CaO-SiO_2$ slags have been measured at 1300°C by a slag-metal-gas equilibrium technique. The experimental zinc oxide activities agree closely with the isoactivity lines calculated on the basis of Toop's ternary integration technique[15] and an estimated entropy of fusion for zinc oxide of 6 E.U.

The calculated excess free energy contours for the $ZnO-CaO-SiO_2$ ternary are similar in shape to those calculated in a similar manner for the $FeO-CaO-SiO_2$ system using Elliott's data on the component binaries[7]. Also the calculated zinc oxide isoactivity figure is similar to the ferrous oxide isoactivity diagram. The zinc oxide isoactivity pattern shows a projection towards the lime orthosilicate composition. This shape is characteristic of FeO, but in the case of ZnO the projection is not so pronounced. Both these observations are in keeping with the slightly more basic behaviour of zinc oxide.

It is felt that the estimated entropy of fusion for zinc oxide is reasonable based on the close agreement between the calculated isoactivity lines and the measured activities and on the similarity between the two ternaries, $ZnO-CaO-SiO_2$ and $FeO-CaO-SiO_2$. In addition, the calculated free energy curve for the $ZnO-SiO_2$ binary agrees quite closely with the free energy curve given by Richardson[8] for this binary based on solid standard states for the two components.

It was found that the solid oxygen electrolyte 0.85 ZrO_2 - 0.15 CaO behaves reversibly at 1300°C over an oxygen potential range of 2.3×10^{-6} to 8.4×10^{-8} atmospheres.

REFERENCES

1. E. N. Bunting, J. Am. Ceram. Soc.; 13, 1 8 (1930).
2. E. R. Segnit, J. Am. Ceram. Soc.; 37, 6 274 (1954).
3. R. C. Bell, G. H. Turner and E. Peters, J. Metals; 6, 472 (1955).
4. A. W. Richards and D. J. Thorne, "Physical Chemistry of Process Metallurgy - Part 1", Interscience, New York, (1961) p. 277.
5. W. G. Davenport, "The Activity of Zinc Oxide in Multi-component Slags", M.A.Sc. Thesis, University of British Columbia, 1960.
6. K. Azuma, S. Goto, O. Ogawa, Nippon Kogyo Kaishi; 81, 18 (1965).
7. J. F. Elliott, J. Metals; 6, 485 (1955).
8. F. D. Richardson, "Physical Chemistry of Melts", Inst. Min. Met., London, (1953) p. 86.
9. C. E. Wicks and F. E. Block, U. S. Bureau of Mines Bulletin 605 (1963).
10. F. Hund, Z. physik. Chem.; 199, 142 (1952).
11. K. Kiukkola and C. Wagner, J. Electrochem. Soc.; 104, 379 (1957).
12. S. P. Mittoff, J. Chem. Phys.; 36, 1383 (1962).
13. B. C. H. Steele and C. B. Alcock, Trans. A.I.M.E.; 233, 1359 (1965).
14. R. Littlewood, Can. Met. Quarterly; 5, 8 (1966).
15. N. J. Olson and G. W. Toop, Trans. A.I.M.E.; 236, 590 (1966).
16. G. W. Toop, Trans. A.I.M.E.; 233, 850 (1965).
17. F. D. Richardson, "The Physical Chemistry of Melts", Inst. Min. Met., London, (1953) p. 93.
18. J. Chipman, Discussion Faraday Soc.; 4, 23 (1948).
19. Hauffe and Wagner, Z. Elektrochem.; 46, 160 (1940).
20. J. A. Kitchener and S. Ignatowitz, Trans Faraday Soc.; 47, 1278 (1951).
21. L. S. Darken and R. W. Gurry, "Physical Chemistry of Metals", McGraw-Hill, New York, (1953) p. 264.
22. W. A. Fischer and W. Ackermann, Archiv. f. d. Eisenhutt.; 9, 643 (1965).

23. E. R. Segnit and J. D. Wolfe, Chem. Eng. Mining Rev.; 45, 215 (1953).

24. R. Schuhmann, Jr., Acta Met.; 3, 223 (1955).

25. R. Schuhmann, Jr., Acta Met.; 3, 220 (1955).

26. J. F. Elliott, M. Gleiser and V. Ramakrishna, "Thermochemistry for Steelmaking, Volume II", Addison-Wesley, Reading, Massachusetts, (1963) p. 578.

27. R. Hargreaves, Journal Institute of Metals; 64, 115 (1939).

28. W. Leitgebel, Z. anorg. Chem.; 202, 305 (1931).

29. A. Schneider and H. Schmid, Z. Elektrochem.; 48, 627 (1942).

30. A. W. Herbenar, C. A. Siebert and O. S. Duffendack, J. of Metals; 2, 323 (1950).

31. L. H. Everett, P. W. M. Jacobs and J. A. Kitchener, Acta Met; 5, 281 (1957).

32. O. Kubaschewski and E. LL. Evans, "Metallurgical Thermochemistry", Pergamon, London, (1965) p. 177.

33. J. Lumsden, "Thermodynamics of Alloys", Institute of Metals, Clowes and Sons, London, (1952) p. 272.

34. O. Kubaschewski and J. A. Catterall, "Thermochemical Data of Alloys", Pergamon, London, (1956) p. 69.

35. Kleppa and King, "Metallic Solid Solutions", W. A. Benjamin Inc., New York, (1965).

36. L. Guttman, Trans. A.I.M.E.; 175, 178 (1948).

37. K. K. Kelly, U. S. Bureau of Mines Bulletin 393 (1936).

38. A. Glassner, A.N.L. - 5750, (1959).

39. M. J. N. Pourbaix and C. M. Rorive-Boute, Discussion Faraday Soc.; 4, 140 (1948).

APPENDIX I

Calculation of Infinitely Dilute Properties of Zinc in the Copper-Zinc System

A. Hargeaves Data[27]

N_{Zn}	a_{Zn}	α_{Zn}
.052	.0045	-5300
.094	.0086	-5720
.144	.0185	-5520
.195	.0301	-5680
.255	.0545	-5430
.373	.134	-5150
.453	.200	-5410
.481	.246	-4920
.504	.291	-4410

B. Leitgebel[28]

T°K	ΔF	N_{Zn}	α_{Zn}
1188	-200	0.883	+7930
1198	-440	0.828	+ 338
1246	-1570	0.707	-8280
1283	-2440	0.577	-5810
1337	-3710	0.441	-4900
1373	-4540	0.381	-5000
1438	-6050	0.273	-4440
1518	-7920	0.191	-4480
1773	-13790	0.063	-4630

C. Schneider and Schmid[29]

T°K	N_{Zn}	a_{Zn}	α_{Zn}
973	0.798	0.80	0
973	0.714	0.57	-5370
973	0.664	0.48	-5570
973	0.580	0.35	-5570
973	0.428	0.14	-6600
1123	0.798	0.795	-2440
7123	0.714	0.612	-4150
1123	0.664	0.531	-4340
1123	0.580	0.398	-4780
1123	0.428	0.184	-5750

D. Herbenar et. al.[30]

Temp.	1073°K	1148°K	1198°K
N_{Cu}	α_{Zn}	α_{Zn}	α_{Zn}
.9465	-5920	-5100	-4780
.8895	-5600	-5230	-5030
.8382	-5570	-5140	-4750
.8001	-5700	-5230	-4840
.7497	-5850	-5270	
.7105	-5530	-4880	

E. Everett, Jacobs and Kitchener[31]

The data of Everett, Jacobs and Kitchener[31] is presented in figure 24. On this figure are drawn the regular solution line used by Davenport and a sloping line which fits the data somewhat better.

F. Kubaschewski and Evans[32]

Their book gives a curve for the integral heats of formation of Cu-Zn alloys based on several techniques. Taking the slope of this line at Zn=0 gives $\overline{\Delta H}$. From this must be subtracted the heat of fusion of zinc, 1760 cals/gm atom. This gives:

$$\overline{\Delta H} = -9160 \text{ cals atom}^{-1}$$

G. Excess Free Energy Expression

Results from all available sources is given in figure 24. The equation of the line drawn for the excess free energy is:

$$\overline{\Delta F}_{Zn}^{xs} = -8200 + 2.58\ T.$$

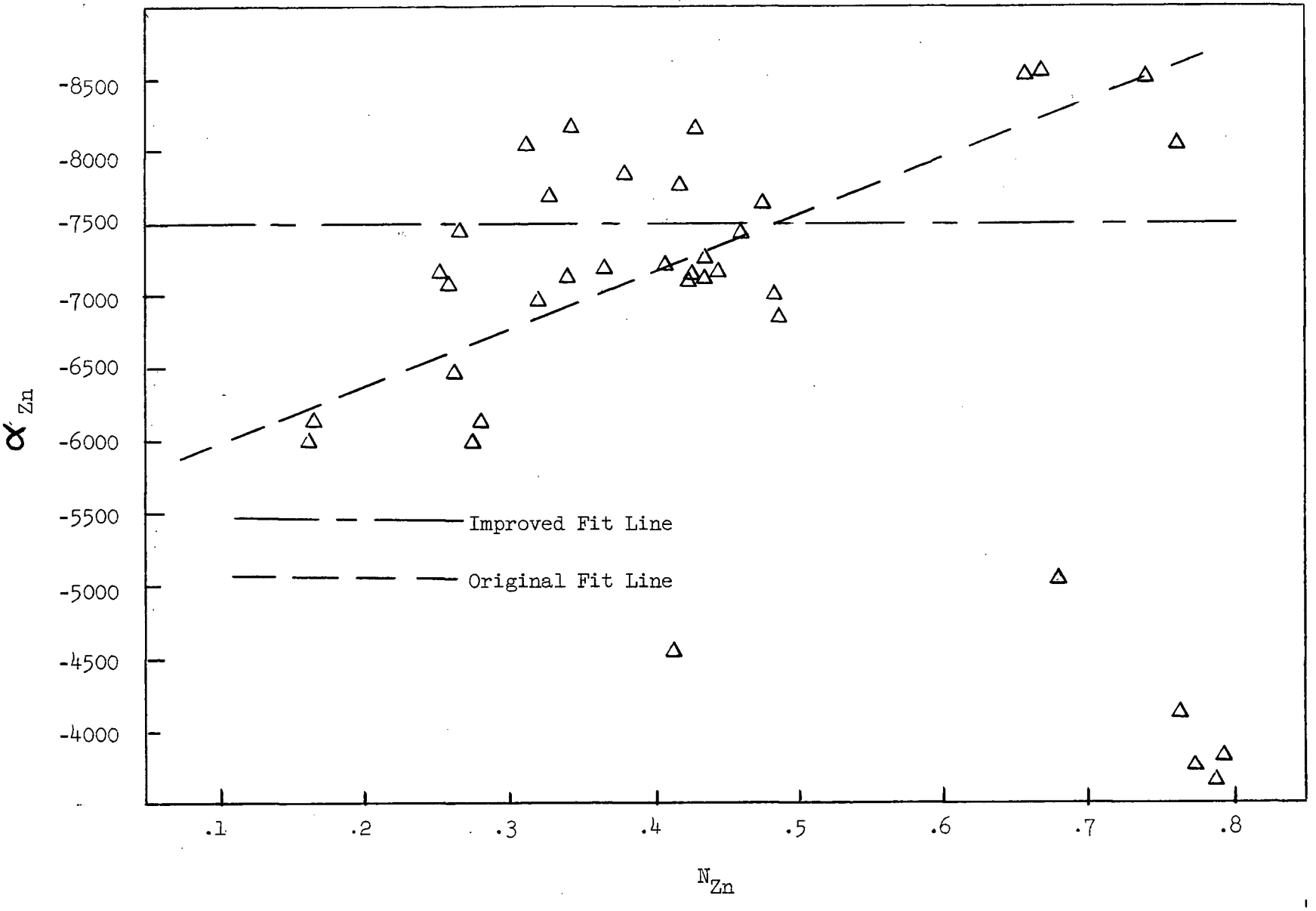

Figure 24. Data of Everett, Jacobs and Kitchener[31].

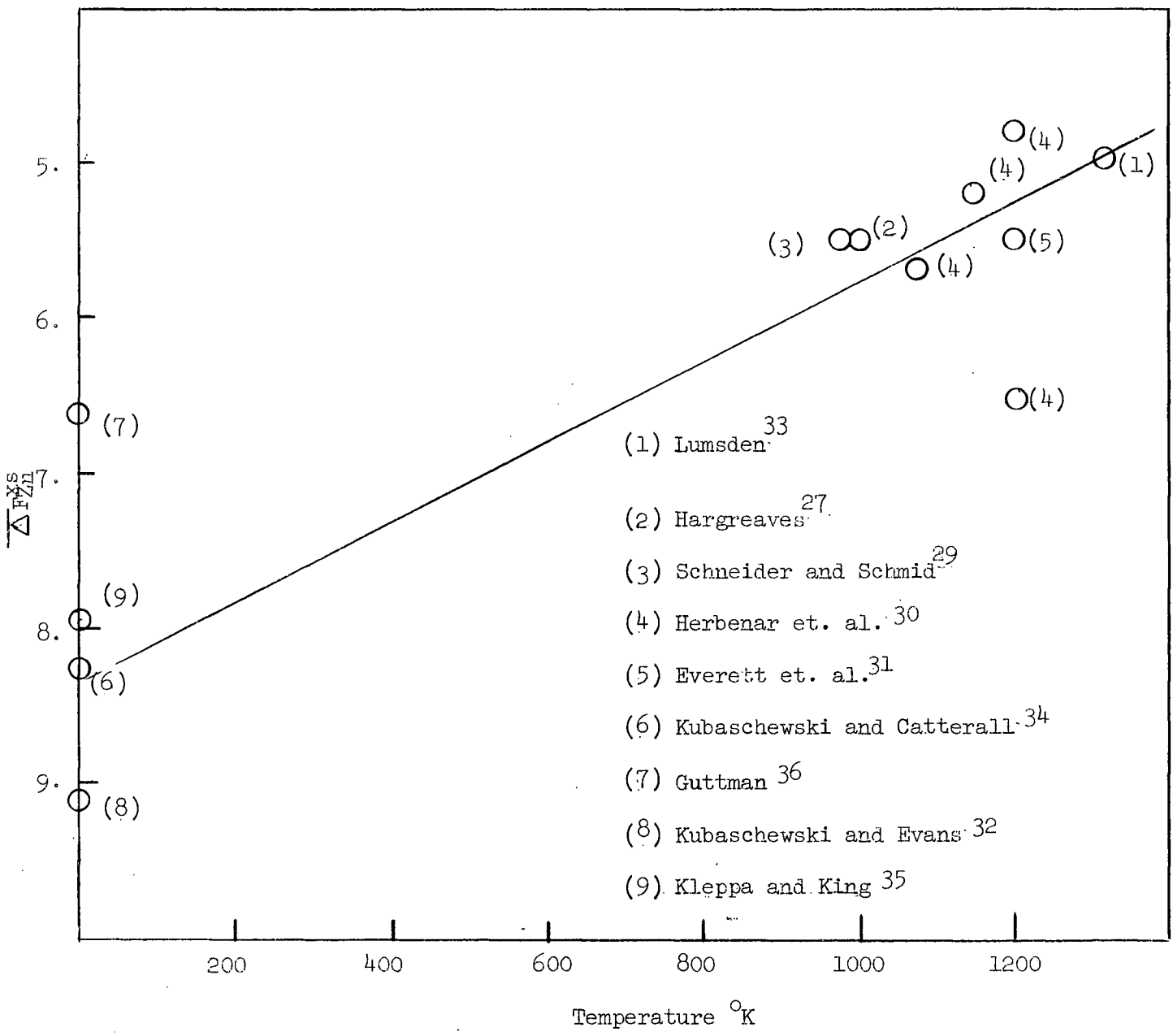

Figure 25. Thermodynamic Data on the Infinitely Dilute Free Energy of Zinc in Copper.

APPENDIX II

The System $ZnO-SiO_2$

A. Previous Work

1.) K.K. Kelly [37]

From Bunting's data[1], Kelly plotted $RlnN_{ZnO}$ as a function of reciprocal temperature and derived a value for ΔH_f from the slope of this line of 4480 cals mol^{-1} (37). From figure 26 it is seen that Bunting's measured compositions do not lie exactly on a line joining the eutectic at 76.5 mol % ZnO with pure ZnO. In fugure 27 values from the linear plot and Bunting's actual values are plotted. Kelly's value lies in between. The error probably lies in the fact that the range of temperature covered is only 22 percent of the temperature difference between the melting point of pure ZnO and the eutectic. Kelly's value gives an entropy of fusion for ZnO of 1.99 E.U. [37]

2.) Richards and Thorne [4]

Richards and Thorne used an entropy of fusion of 5 E.U.[4] There was no reference given as to the source of this value.

3.) Glassner [38]

Glassner gives a difference in enthalpy between solid and liquid zinc oxide at 2248°K of 8600 cals[38]. This value is presumably calculated from heat capacity considerations. This enthalpy gives an entropy of fusion for ZnO of 3.8 E.U.

4.) Davenport [5]

Based on a somewhat arbitrary closure of his α plot for SiO_2 in the $ZnO-SiO_2$ binary[5], Davenport derived a value for the entropy of fusion for ZnO of 2.85 E.U.[5] He used much the same technique as was used in the present study.

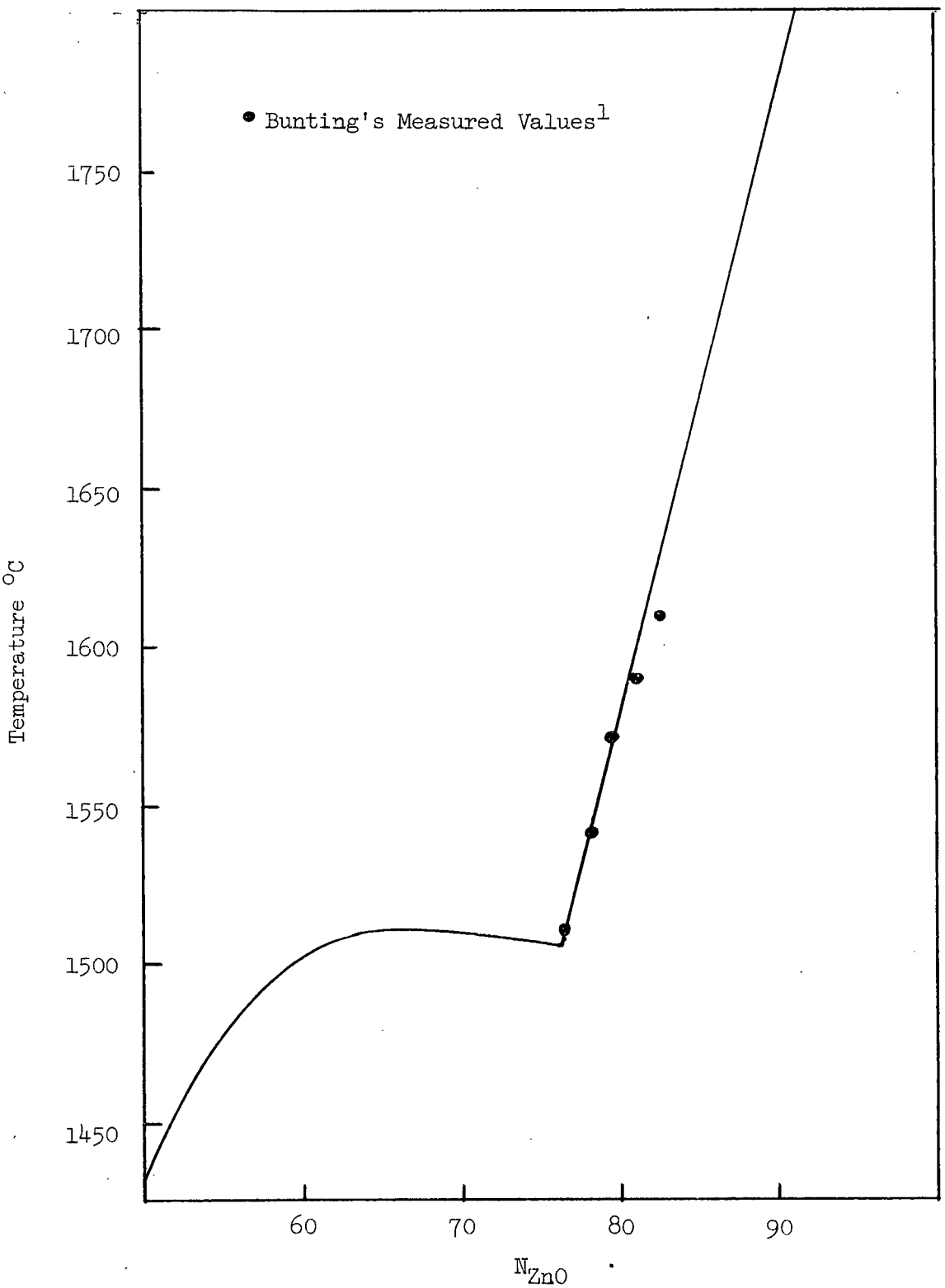

Figure 26. ZnO-Rich Side of $ZnO-SiO_2$ Binary.[1]

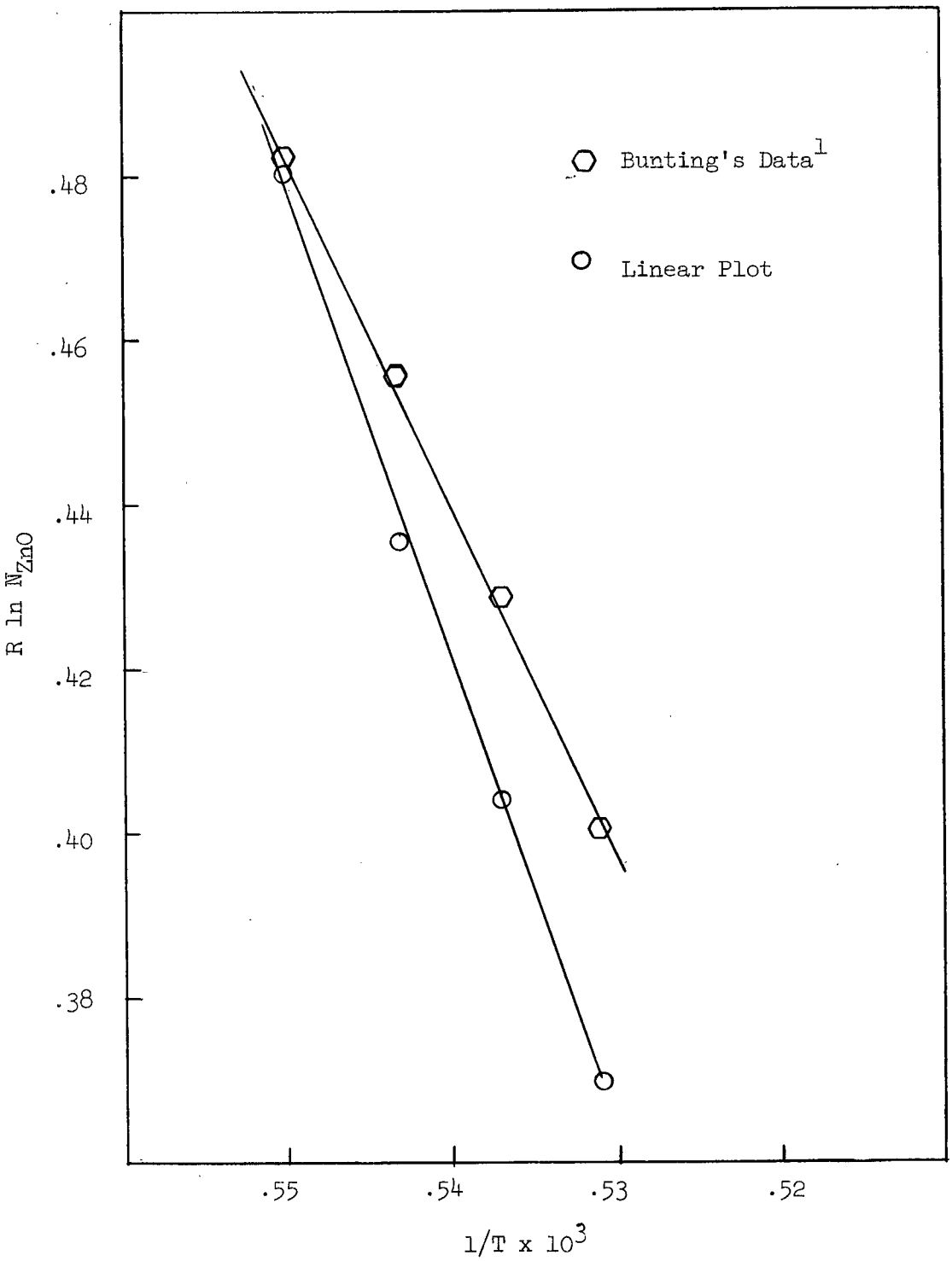

Figure 27. Estimate of Enthalpy of Fusion for ZnO from the Liquidus Line.

B. Estimation of ΔS_f ZnO

Elliott[26] has plotted activities calculated from Richardson's free energy curve[8] for the ZnO-SiO_2 binary. These activities from N_{ZnO} = 0.765 (the eutectic between Zn_2SiO_4 and ZnO) to saturation at 1600°C may be used together with Bunting's phase diagram[1] to satisfy the formula used in Chipman's melting point depression expression[18] to derive an average value for the entropy of fusion for ZnO. This is shown in table 3. The first composition (N_{ZnO} = 0.807) is not very useful as the liquidus is not well established at this point. The average of the other two points is taken as 6 E.U.

Table III

Calculation of ΔS_f ZnO

Chipman's Liquidus Curve Expression: [18]

$$\Delta S_f = \frac{-RT\ln a_{ZnO}}{T-Tm_{ZnO}}$$

N_{ZnO}	ΔT	$a_{1600°C}$*	$\gamma_{1600°C}$	γ_T	a_T	$\ln a_T$	ΔF	ΔS_f
.807	18	.96	1.188	1.189	.96	-.0407	-151	8.3
.783	55	.91	1.16	1.165	.912	-.0918	-331	6.02
.772	75	.85	1.10	1.144	.883	-.124	-442	5.9

C. Calculation of Activity for Silica to N_{SiO_2} = 0.235

Silica activity may be calculated from the phase diagram using the techniques developed by Chipman[18] and Hauffe and Wagner[19](Table 4).

*From Elliott[26]

Table IV

Activity of SiO_2 from $N_{SiO_2} = 1.0$ to $N_{SiO_2} = 0.235$

1. Congruent melting Compound Method[19]

Symbols: H_f = Heat of fusion of Zn_2SiO_4 = 18.7 kcals mol^{-1}
Θ = Melting Point of Zn_2SiO_4 = 1784°K
x_{ZnO} = 0.666
x_{SiO_2} = 0.333 Mol fractions in Zn_2SiO_4
T = Liquidus temperature
N_{ZnO}, N_{SiO_2} = Composition

$$RT\ln a^{II}_{SiO_2} = RT\ln a^{I}_{SiO_2} + \frac{\Delta H_f}{\Theta}\left[\frac{N_{ZnO}(\Theta-T)}{N_{SiO_2}-X_{SiO_2}} + X_{ZnO}\int_{X_{SiO_2}}^{N_{SiO_2}} \frac{(\Theta-T)}{(N-X)^2}_{SiO_2} dN_{SiO_2}\right]$$

N_{SiO_2}	T°K	$(\Theta-T)$	$(N-X)$	$(\Theta-T)/(N-X)^2$	$X_{ZnO}\int_X^N [\,]dN_{SiO_2}$	[PartI]	$\frac{\Delta H_f}{\Theta}[\,]$
.50	1705	80	.166	2900	293	241	5600
.45	1751	34	.116	2520	204	161	3830
.40	1775	10	.066	2290	124	90	2240
.38	1780	5	.046	2360	93	67	1680
.36	1783	2	.026	2940	58	49	1120
.32	1784.5	.5	-.013	2960	-29	-26	-580
.30	1783.5	1.5	-.033	1460	-59	-32	-950
.28	1782.5	2.5	-.053	890	-74	-34	-1120
.26	1781.5	3.5	-.073	650	-85	-36	-1270
.235	1780	5	-.098	520	-95	-39	-1400

The graphical integration of $(\Theta-T)/(N-X)^2$ against N_{SiO_2} is given in figure 28.

2. Liquidus Curve Method[18]

$$\ln a = \frac{T-Tm\triangle S_f}{T \quad R}$$

$\triangle S_f$ = Entropy of Fusion of SiO_2 = 1.8 E.U.[17]

N_{SiO_2}	T°K	T-Tm/T	ln a	a	γ	α_{SiO_2}
.975	1968	-.00913	-.0083	.992	1.018	111000
.95	"	"	"	"	1.044	67200
.90	"	"	"	"	1.102	37800
.85	"	"	"	"	1.166	26600
.80	"	"	"	"	1.241	21100
.75	"	"	"	"	1.321	17400
.70	"	"	"	"	1.418	15100
.657	"	"	"	"	1.51	13600
.65	1951	-.0179	-.0163	.984	1.51	12900
.60	1853	-.0718	-.0652	.937	1.56	10200
.55	1773	-.1200	-.1093	.896	1.63	8480
.50	1705	-.165	-.150	.86	1.72	7330
.45	1751		-.705	.493	1.095	1040
.40	1775		-1.172	.309	.773	-2510
.36	1783		-1.492	.223	.62	-4080
.30	1783.5		-2.065	.126	.420	-6230
.26	1781.5		-2.17	.113	.435	-5330
.235	1780		-2.207	.109	.464	-4590

D. Calculation of Activity for ZnO to $N_{ZnO} = 0.50$

The same techniques may be used to calculate activities for ZnO from the phase diagram utilizing the estimated entropy of fusion of 6 E.U.

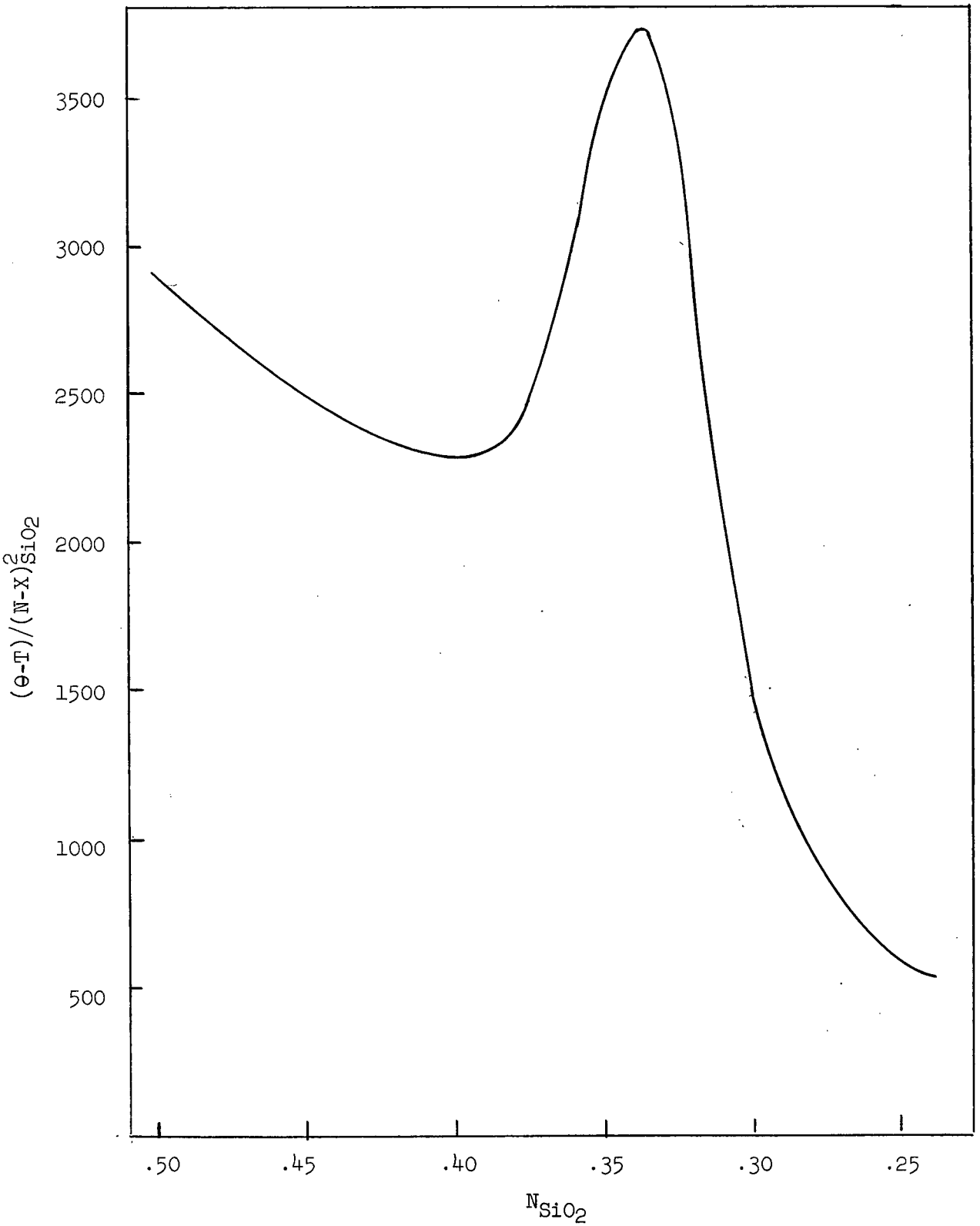

Figure 28. Graphical Integration of the Liquidus Curve of Zn_2SiO_4.

Table V

Activity of ZnO from $N_{ZnO} = 1.0$ to $N_{ZnO} = 0.5$

1. Congruent Melting Compound Method[19]

N_{ZnO}	$T^{o}K$	$(\Theta-T)$	$(N-X)$	$(\Theta-T)/(N-X)^2$	$X_{SiO_2}\int_{X}^{N}[\ ]\,dN_{ZnO}$	[Part I]	$\frac{\Delta H_f}{\Theta}[\ ]$
.765	1780	5	.098	520	47	12	618
.74	1781.5	3.5	.073	654	42	12	566
.72	1782.5	2.5	.053	890	37	14	524
.70	1783.5	1.5	.033	1460	30	14	461
.68	1784.5	.5	.013	2960	15	12	283
.64	1783.5	2	-.026	2940	-29	-28	-597
.62	1780	5	-.046	2360	-47	-41	-922
.60	1775	10	-.066	2290	-62	-60	-1280
.55	1751	34	-.116	2520	-102	-132	-2450
.50	1705	80	-.166	2900	-147	-241	-4070

2. Liquidus Curve Method[18]

N_{ZnO}	$T^{o}K$	T-Tm/T	$\ln a$	a	γ	α_{ZnO}
.95	2148	-.0465	-.141	.868	.913	-160000
.90	2048	-.0977	-.296	.743	.825	-78000
.85	1948	-.1540	-.467	.626	.737	-52200
.80	1848	-.2170	-.657	.517	.647	-39700
.765	1780	-.2630	-.797	.45	.588	-33600
.74	1781.5		-.812	.458	.62	-24700
.70	1783.5		-.842	.43	.615	-19000
.64	1783.5		-1.141	.351	.55	-16100
.60	1775		-1.336	.261	.435	-18200
.55	1751		-1.678	.185	.337	-18500
.50	1705		-2.176	.112	.224	-17400

E. Gibbs Duhem Integration

The Duhem-Margules Equation[21] may be written as:

$$\alpha_{ZnO} = \frac{1}{(N_{SiO_2})^2}\int_0^{N_{SiO_2}} \alpha d N_{SiO_2} - \frac{N_{ZnO}\alpha_{SiO_2}}{N_{SiO_2}}$$

Table VI

SiO_2-ZnO Binary Integration

N_{SiO_2}	α_{SiO_2}	Part I	Part II	α_{ZnO}	α_{ZnO}*	N_{ZnO}
.02	-24400	-1400000	-1195000	-205000	-205000	.98
.05	-15800	-460000	-300000	-160000	-160000	.95
.10	-11000	-178000	-99000	-78400	-78000	.90
.15	-8000	-99200	-45200	-54000	-52000	.85
.20	-6000	-64500	-24000	-40500	-40000	.80
.25	-6000	-46000	-18000	-28000	-28000	.75
.30	-6000	-35400	-14000	-21400	-20000	.70
.35	-5000	-27800	- 9250	-18550	-17000	.65
.40	-3000	-22700	- 4500	-18200	-18000	.60
.45	1000	-18200	1100	-19300	-18000	.55
.50	4000	-14000	4000	-18300	-18000	.50
.60	10000	-7850	6670	-14500		.40
.70	14000	-3310	6000	-9300		.30
.80	21000	195	5250	-5050		.20
.90	38000	3550	4230	-680		.10
.95	67000	6100	3530	2570		.05

*From Table V.

The resulting α plots are given in figure 29.

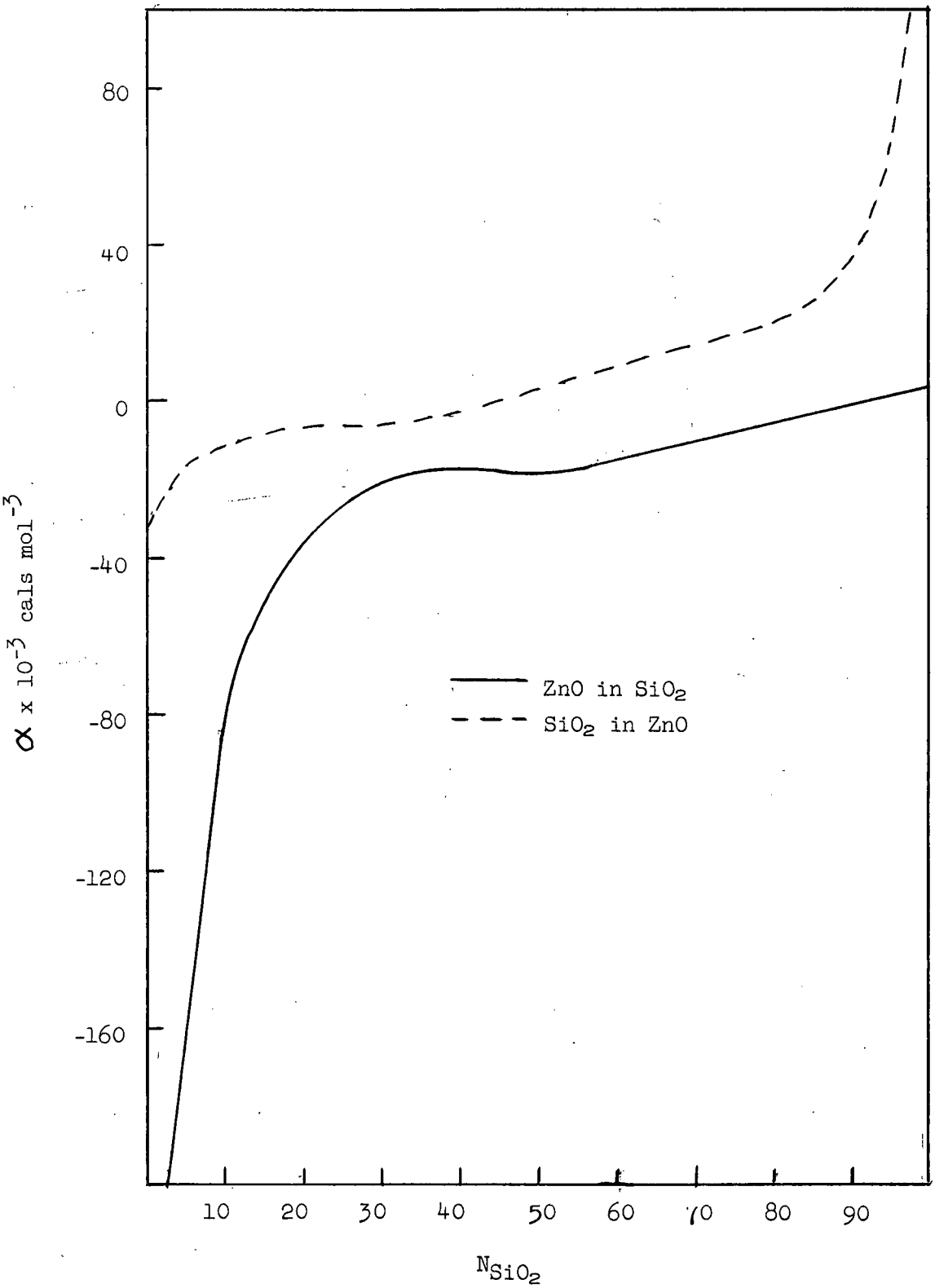

Figure 29. α Plots for ZnO-SiO_2 Binary.

F. Excess Free Energy Curve

Table VII

Excess Free Energy of $ZnO-SiO_2$ at 1600°C

N_{ZnO}	ΔF^{xs}
.05	227
.10	280
.15	155
.20	-37
.25	-265
.30	-555
.35	-892
.40	-1260
.45	-1593
.50	-1750
.55	-1927
.60	-2064
.65	-2064
.70	-2048
.75	-2257
.80	-2166
.85	-1781
.90	-1584
.95	-408

Based on the metastable liquid standard states and calculated from the α curves by the method shown in Appendix III.

G. Comparison with Richardson's Free Energy Curve[8]

Richardson's free energy curve for the binary $ZnO-SiO_2$ with respect to the solid standard states of the two components[8] is shown in figure 30. In the same figure the standard states are changed to the two pure liquids and the resulting curve compared to that calculated in the previous section. The agreement is quite good.

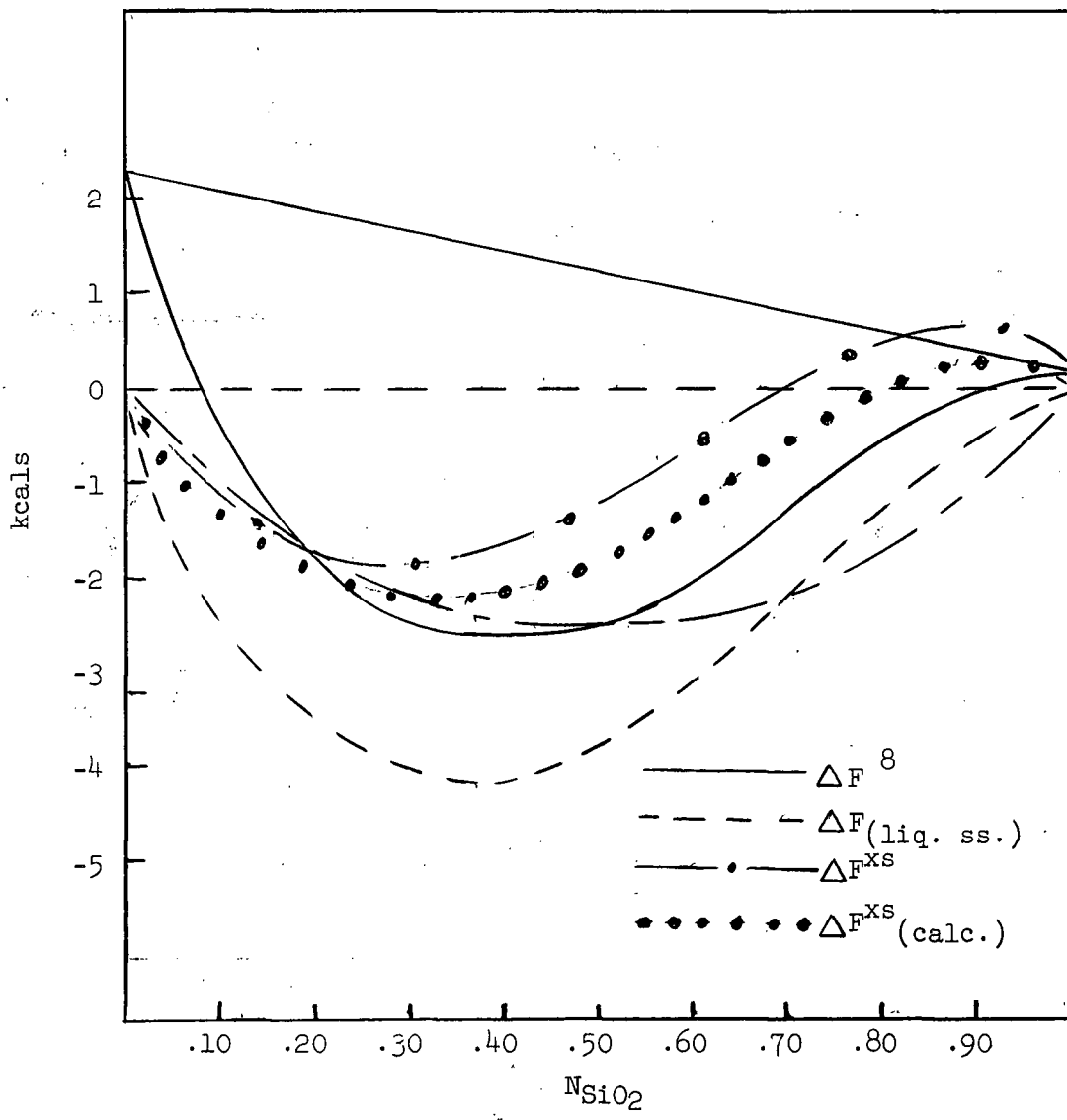

Figure 30. Comparison Between the Free Energy of the $ZnO-SiO_2$ Binary at 1600°C as given by Richardson[8] and as derived in the Present Study.

APPENDIX III

Toop's Ternary Integration Technique

The location and definition of terms used in this derivation are shown in figure 31. Toop gives the following expression for the excess free energy within the ternary:[15]

$$\Delta F^{xs}_{tern} = (1-N_3)^2 \left[\Delta F^{xs}_{2-1}\right]_{N_1/N_2} + (1-N_1)^2 \left[\Delta F^{xs}_{2-3}\right]_{N_2/N_3} + (1-N_2)^2 \left[\Delta F^{xs}_{1-3}\right]_{N_1/N_3}.$$

The excess free energy in a binary system is given by:

$$\begin{aligned}\Delta F^{xs} &= RT(N_1 \ln \gamma_{1(2)} + N_2 \ln \gamma_{2(1)}) \\ &= N_1(1-N_1)^2 \alpha_{1(2)} + N_2(1-N_2)^2 \alpha_{2(1)} \\ &= N_1 N_2 (N_2 \alpha_{1(2)} + N_1 \alpha_{2(1)})\end{aligned}$$

Thus by using the values of all three ordinates of any one point, the excess free energy at that point may be calculated by using the binary α plots.

The log of the activity coefficient of a component within a ternary is given by the following expression:[16]

$$\text{Log}\,\gamma_{2(tern)} = \left[\frac{N_1}{1-N_2}\,\text{Log}\,\gamma_{2(1)} + \frac{N_3}{1-N_2}\,\text{Log}\,\gamma_{2(3)}\right]_{N_2} - (1-N_2)^2 \left[\Delta F^{xs}_{1-3}\right]_{N_1/N_3}$$

$$\text{Log}\,\gamma_{2(tern)} = \frac{1}{RT}\Big\langle \left[N_1(1-N_2)\alpha_{2(1)} + N_3(1-N_2)\alpha_{2(3)}\right]_{N_2} + (1-N_2)^2 \left[N_1 N_3 (N_1 \alpha_{3(1)} + N_3 \alpha_{1(3)})\right]_{N_1/N_3} \Big\rangle .$$

$$\alpha_{2(tern)} = N_2 e^{\text{Log}\,\gamma_{2(tern)}}$$

The α plots of the binary systems $CaO\text{-}SiO_2$ and $FeO\text{-}SiO_2$ are included (Figures 32 and 33 respectively).

APPENDIX III

Toop's Ternary Integration Technique

The location and definition of terms used in this derivation are shown in figure 31. Toop gives the following expression for the excess free energy within the ternary:[15]

$$\Delta F^{xs}_{tern} = (1-N_3)^2 \left[\Delta F^{xs}_{2-1}\right]_{N_1/N_2} + (1-N_1)^2 \left[\Delta F^{xs}_{2-3}\right]_{N_2/N_3} + (1-N_2)^2 \left[\Delta F^{xs}_{1-3}\right]_{N_1/N_3}.$$

The excess free energy in a binary system is given by:

$$\begin{aligned}\Delta F^{xs} &= RT(N_1 \ln \gamma_{1(2)} + N_2 \ln \gamma_{2(1)}) \\ &= N_1(1-N_1)^2 \alpha_{1(2)} + N_2(1-N_2)^2 \alpha_{2(1)} \\ &= N_1 N_2 (N_2 \alpha_{1(2)} + N_1 \alpha_{2(1)})\end{aligned}$$

Thus by using the values of all three ordinates of any one point, the excess free energy at that point may be calculated by using the binary α plots.

The log of the activity coefficient of a component within a ternary is given by the following expression:[16]

$$\text{Log}\,\gamma_{2(tern)} = \left[\frac{N_1}{1-N_2}\,\text{Log}\,\gamma_{2(1)} + \frac{N_3}{1-N_2}\,\text{Log}\,\gamma_{2(3)}\right]_{N_2} - (1-N_2)^2 \left[\frac{\Delta F^{xs}_{1-3}}{RT}\right]_{N_1/N_3}$$

$$\text{Log}\,\gamma_{2(tern)} = \frac{1}{RT}\Big\langle \left[N_1(1-N_2)\alpha_{2(1)} + N_3(1-N_2)\alpha_{2(3)}\right]_{N_2} + (1-N_2)^2 \left[N_1 N_3 (N_1 \alpha_{3(1)} + N_3 \alpha_{1(3)})\right]_{N_1/N_3} \Big\rangle .$$

$$\alpha_{2(tern)} = N_2 e^{\text{Log}\,\gamma_{2(tern)}}$$

The α plots of the binary systems $CaO\text{-}SiO_2$ and $FeO\text{-}SiO_2$ are included (Figures 32 and 33 respectively).

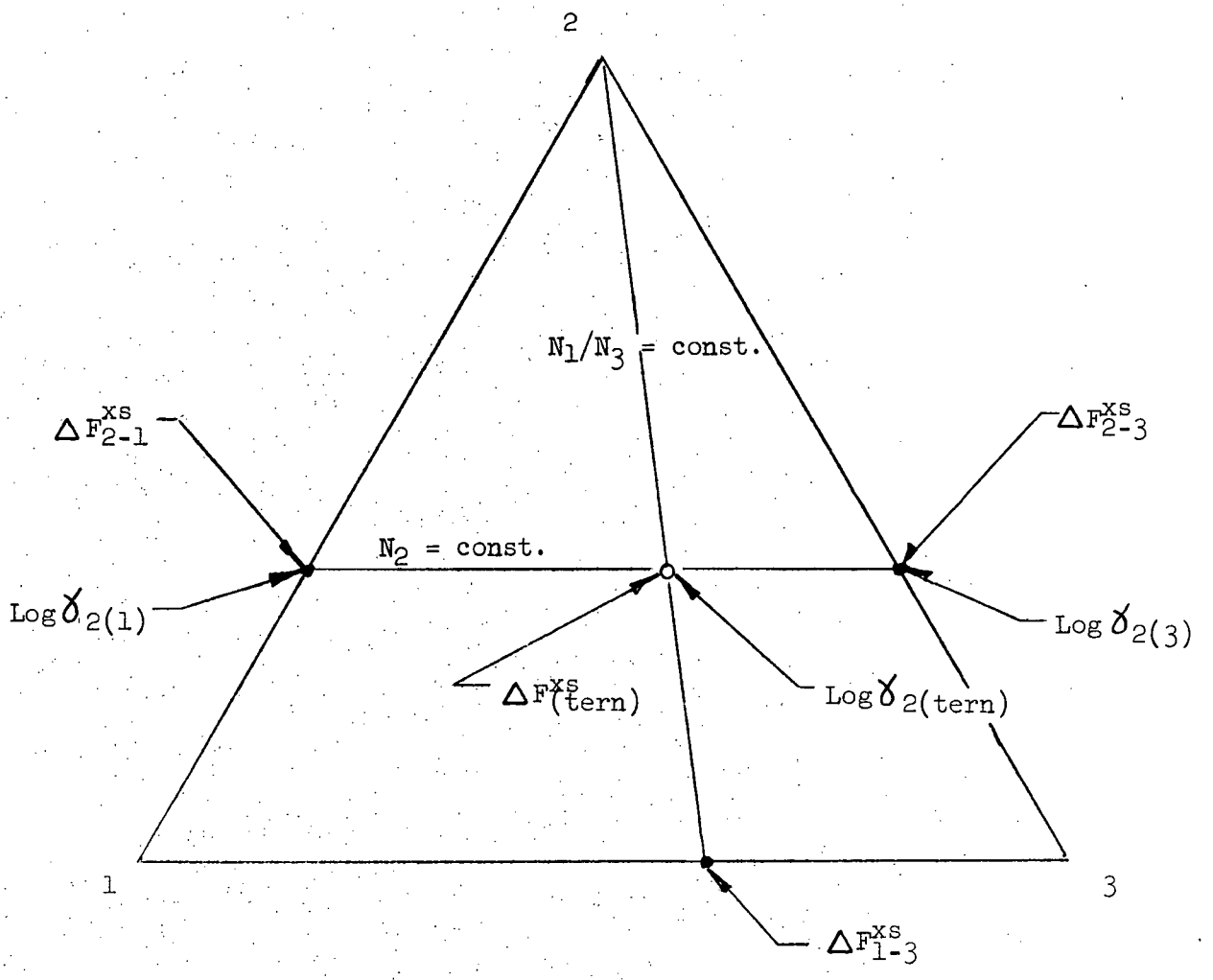

Figure 31. Definition and Location of Terms Used in Appendix III.[15]

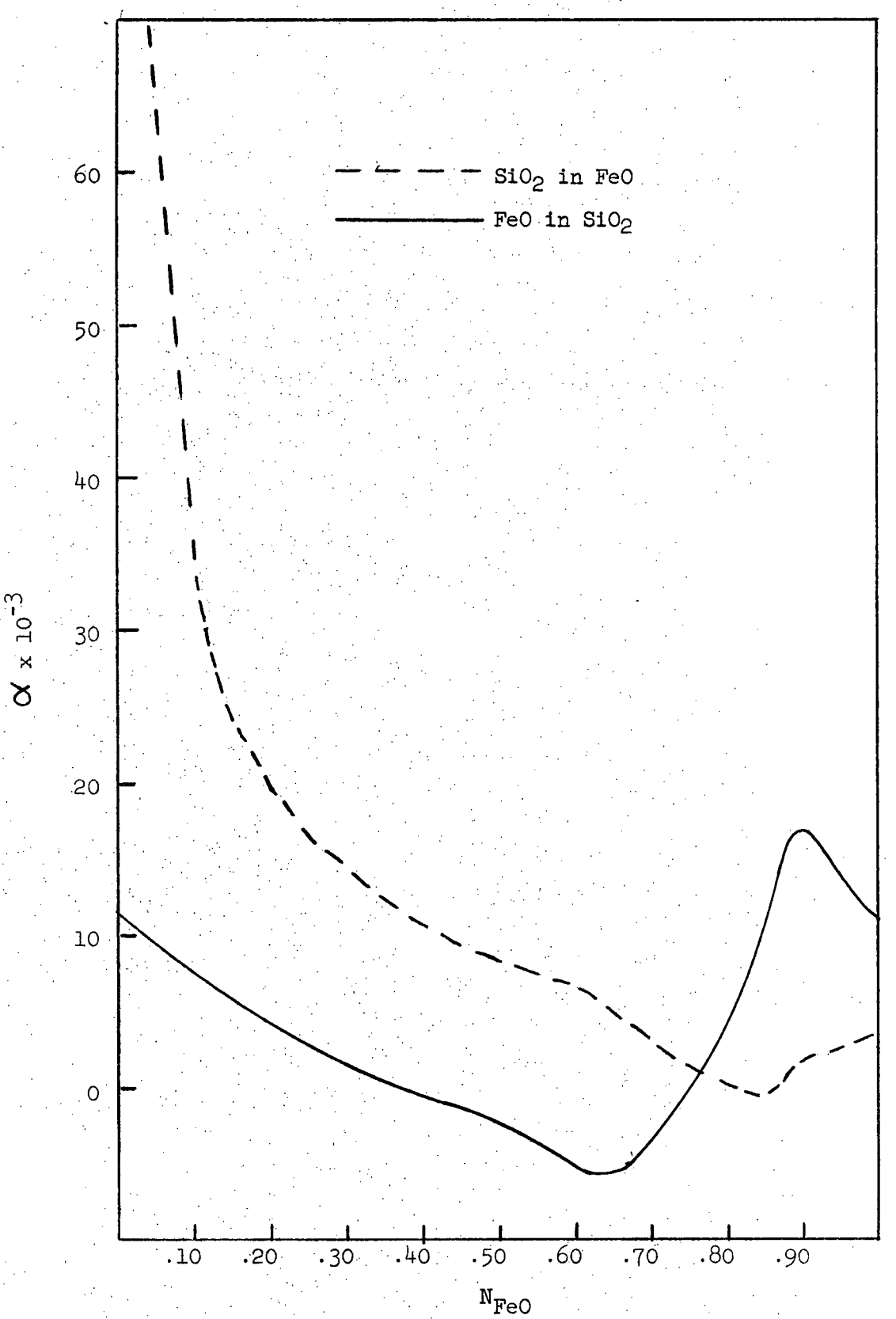

Figure 32. α Plots for the FeO-SiO_2 Binary.

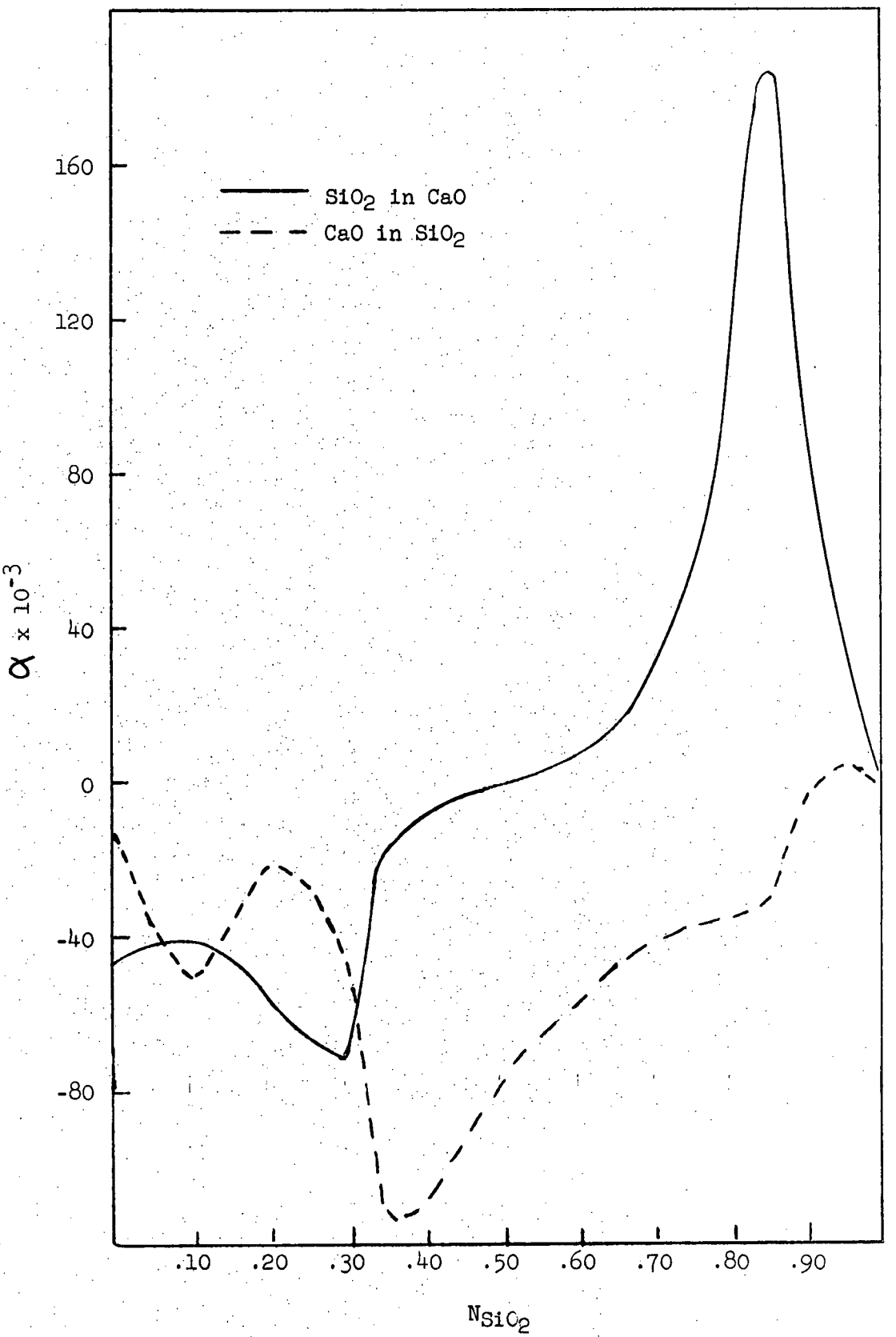

Figure 33. α Plots for the CaO-SiO_2 Binary.

APPENDIX IV

Oxygen Potential Limits

A. 1300°C

1.) Lower Limit

$$Zn_{(l)} \longrightarrow Zn_{(g)}$$

$$0 = \frac{-6275}{T} + 5.33 - \text{Log } P_{Zn} \quad [39]$$

$$\frac{a_{Zn(g)}}{a_{Zn(l)}} = 22$$

$$a_{Zn(l)} \leq 0.0455$$

$$[a_{Zn}] (P_{O_2})^{\frac{1}{2}} = 7.3 \times 10^{-7} \quad (9)$$

$$P_{O_2} \geq 2.6 \times 10^{-10}$$

2.) Upper Limit

$$2Cu + \tfrac{1}{2}O_2 \rightleftharpoons Cu_2O \qquad \Delta F_{1573^\circ K} = -14200 \text{ cals.}$$

For unit activity of Cu_2O at 1300°C

$$PP\ O_2 = 1.1 \times 10^{-4}$$

B. 1600°C

$$\frac{a_{Zn(g)}}{a_{Zn(l)}} = 78$$

$$P_{O_2} \geq 4.5 \times 10^{-5}$$

$$4Cu + O_2 \longrightarrow 2Cu_2O \qquad K_{1873^\circ K} = 1.38 \times 10^{-3} \quad (9)$$

$$Cu_2O \geq 0.18$$

APPENDIX V

Free Energy of Formation of Zn_2SiO_4

The slag used in runs I and J was saturated in both ZnO and Zn_2SiO_4. This indicates that this slag may be used to determine the free energy of formation of Zn_2SiO_4 at 1300 C.

The calculated value for the silica activity at this point is approximately $a_{SiO_2} = 0.2$. The standard state may be changed from liquid to solid by the following expression based on an entropy of fusion for SiO_2 of 1.8 E.U.:

$$\frac{a_{ZnO(l)}}{a_{ZnO(s)}} = \frac{1560}{T} - 0.91$$

hence $a_{SiO_2(s)}$ 1600 C = .22

and $a_{SiO_2(s)}$ 1300 C = .20

using the regular solution theory temperature adjustment.

For the free energy of formation of Zn_2SiO_4

$$K = \frac{[ZnO]^2 [SiO_2]}{[Zn_2SiO_4]} = 0.2$$

$$\triangle F \text{ 1300 C} = (1.98)(1573) \ln (.20)$$

$$= -5000 \text{ cals.}$$

Kitchener and Ignatowicz[20] give the following expression for the free energy of formation of Zn_2SiO_4.

$$\triangle F = -7129 + 0.23\ T$$
$$\triangle F 1300 \text{ C} = -6800 \text{ cals.}$$

In view of the rather large estimate of error in $\triangle H^\circ$ and $\triangle S^\circ$ quoted in Kitchener and Ignatowicz's paper, the agreement is quite good.